Formation of magnesium-smectite during lacustrine carbonates early diagenesis: Study case of the volcanic crater lake Dziani Dzaha (Mayotte – Indian Ocean)

Vincent Milesi, Didier Jézéquel, Mathieu Debure, Pierre Cadeau, Francois Guyot, Gérard Sarazin, Francis Claret, Emmanuelle Vennin, Carine Chaduteau, Aurélien Virgone, et al.

FORMATION OF MG-SMECTITE DURING LACUSTRINE CARBONATES EARLY DIAGENESIS: STUDY CASE OF THE VOLCANIC CRATER LAKE DZIANI DZAHA (MAYOTTE – INDIAN OCEAN)

V. MILESI[*1], D. JEZEQUEL[1], M. DEBURE[3], P. CADEAU[1], F. GUYOT[2], G. SARAZIN[1], F. CLARET[3], E. VENNIN[4], C. CHADUTEAU[1], A. VIRGONE[5], E.C. GAUCHER[5], M. ADER[1]

[*]Corresponding author: vmilesi@asu.edu
[1]Institut de Physique du Globe de Paris, Sorbonne Paris Cité, Univ Paris Diderot, UMR 7154 CNRS, F-75005 Paris, France
[2]IMPMC, Sorbonne Université, MNHN, Paris, France
[3]BRGM, French Geological Survey, Orléans, France
[4]Bourgogne University, Dijon, France
[5]Total, EP CSTJF, Pau, France

Abstract

The volcanic crater lake of Dziani Dzaha in Mayotte is studied to constrain the geochemical settings and the diagenetic processes at the origin of Mg-phyllosilicates associated with carbonate rocks. The Dziani Dzaha is characterized by an intense primary productivity, volcanic gases bubbling in three locations and a volcanic catchment of phonolitic/alkaline composition. The lake water has an alkalinity of ~0.2 $mol \cdot L^{-1}$ and pH values of ~9.3. Cores of the lake sediments reaching up to one meter in length were collected and studied by means of CHN elemental analyzer, X-ray fluorescence spectrometry and X-ray powder diffraction. In surface sediments, the content of total organic carbon reaches up to 35wt.%. The mineral content consists of aragonite and hydromagnesite with minor amounts of alkaline feldspar and clinopyroxene from the volcanic catchment. Below 30cm deep, XRD analyses of the <2 µm clay fraction indicate the presence of a saponite-like mineral, a Mg-rich smectite. The saponite-like mineral accumulates at depth to reach up to ~25wt.%, concurrent with a decrease of the contents of hydromagnesite and organic matter. Thermodynamic considerations and mineral assemblages suggest that the evolution of the sediment composition resulted from early diagenetic reactions. The formation of the saponite-like mineral instead of Al-free Mg-silicates resulted from high aluminum availability, which is favored in restricted lacustrine environments hosted in alkaline volcanic terrains commonly emplaced during early stages of continental rifting. Supersaturation of the lake water relative to saponite is especially due to high pH values, themselves derived from high primary productivity. This suggests that a genetic link may exist between saponite and the development of organic-rich carbonate rocks, which may be fueled by the input of CO_2-rich volcanic gases. This provides novel insights into the composition and formation of saponite-rich deposits under specific geodynamic context such as the Cretaceous South Atlantic carbonate reservoirs.

Keywords: lacustrine carbonates, early diagenesis, saponite, volcanic lake, authigenesis, organic matter decomposition, magnesian clays

1. Introduction

Mg-rich clay minerals, referred hereafter as Mg-silicates, are increasingly reported associated with ancient and modern carbonates rocks (*e.g.*, Hover *et al.*, 1999; Bristow *et al.*, 2009; Wright, 2012; Zeyen *et al.*, 2015, 2017; Pace *et al.*, 2016; Gérard *et al.*, 2018). In particular, Mg-silicates have been reported in lacustrine carbonate reservoirs of the South-Atlantic (*e.g.*, Bertani and Carozzi, 1985a, 1985b; Rehim *et al.*, 1986; Wright, 2012) and their dissolution during diagenesis was proposed to explain the high porosity of these carbonate rocks (Wright and Barnett, 2015; Tosca and Wright, 2015). These phases seem to form either through direct precipitation from water or during very early diagenesis (*e.g.*, Tosca, 2015) and record specific chemical conditions, especially high pH values. Thus, they have a strong potential to help in palaeoenvironmental reconstruction of continental carbonates deposits and their evolution through the diagenesis (Chamley, 1989; Weaver, 1989; Bristow *et al.*, 2009).

The variety of geologic environments allowing Mg-rich clays to form is unclear. In Phanerozoic rocks, the presence of Mg-silicates has been attributed to different depositional environments including weathering profiles developed on Mg-rich rocks such as basic or ultrabasic igneous rocks (Huang *et al.*, 2013), hydrothermal settings where fluids interact with Mg-rich igneous material (Setti *et al.*, 2004), alkaline lakes and evaporative basins (Van Denburgh, 1975; Yuretich and Cerling, 1983; Darragi and Tardy, 1987; Banfield *et al.*, 1991; Hay *et al.*, 1991; Hover *et al.*, 1999; Martini *et al.*, 2002; Bristow *et al.*, 2009; Zeyen *et al.*, 2015, 2017; Pace *et al.*, 2016; Gérard *et al.*, 2018). Spring inflows into lakes hosted in basic volcanic terrains could also contribute to create the right set of conditions, *i.e.*, high carbonate alkalinity, high Si, Mg and Ca concentrations, for the development of lacustrine carbonates associated with Mg-silicates (Wright, 2012). The Doushantuo carbonate formation, which hosts fossil records of the early Ediacaran period (635 – 551 Ma), illustrates the controversy about the formation of Mg-rich clays. In this carbonate formation, the presence of saponite, a Mg- and Al-rich smectite, was interpreted as either an early diagenetic phase formed *in situ* in an alkaline and non-marine environment (Bristow *et al.*, 2009), or as a detrital phase resulting from local to regional weathering of adjacent continental areas dominated by mafic to ultramafic volcanic rocks (Huang *et al.*, 2013). In this respect, the aluminum content of Mg-silicates may be of key interest for such reconstructions as it has been proposed to provide insights into the nature and the amounts of detrital silicate inputs in lacustrine environments (*e.g.*, Millot, 1970).

Present-day sedimentary features can inform on the palaeoenvironments where Mg-rich clays formed. Sediments developed in lakes characterized by waters with high pH (>9), and either relatively high silica concentrations (Van Denburgh, 1975; Yuretich and Cerling, 1983; Darragi and Tardy, 1987; Banfield *et al.*, 1991; Hay *et al.*, 1991; Zeyen *et al.*, 2015, 2017; Gérard *et al.*, 2018) or high magnesium concentrations (Hover *et al.*, 1999; Martini *et al.*, 2002), were found to host Mg-silicates.

To date, however, the specific geochemical conditions controlling their formation remain unclear. In particular, the role of volcanic catchment and spring inflow is uncertain, limiting palaeoenvironmental and early diagenesis interpretations. To tackle this issue, the tropical volcanic crater lake Dziani Dzaha in Mayotte (Indian Ocean) was chosen as a possible palaeoenvironmental analogue for the formation model of Mg-rich silicates associated with continental carbonates. The lake waters are known to be alkaline and the catchment is composed of volcanic rocks of phonolitic/alkaline composition. Mg-silicate minerals were recently identified in the stromatholites of the lake (Gérard *et al.*, 2018), suggesting that they may also be present in the soft carbonated sediments. The mineralogy of the first meter of the sediment column was studied to identify possible occurrences of Mg-silicates and provide insights on the processes leading to the formation of carbonates associated with Mg-silicates during early diagenesis.

2. Geologic setting and limnology of the Dziani Dzaha

The Dziani Dzaha (meaning volcanic crater lake in Mahorian) is a tropical volcanic crater lake located in the island complex of Mayotte in the Northern Mozambique Channel. Mayotte is the most southern and oldest island complex of the Comoros Archipelago. The initial volcanism period is estimated to ~ 15-10 Ma (Nougier *et al.*, 1986); however, the Mayotte complex island has displayed a late volcanic activity for the last 2.5Ma (Pelleter *et al.*, 2014). The alkaline volcanism at the origin of the Comoros Archipelago was suggested as deriving from the partial melt of lithospheric mantle metasomatized by CO_2-rich fluids beneath an ocean-continent transitional crust (Nougier *et al.*, 1986; Mougenot *et al.*, 1989; Bertil and Reynoult, 1998; Coltorti *et al.*, 1999; Pelleter *et al.*, 2014). Mayotte is made of two main volcanic islands: Grande Terre and Petite Terre (Fig. 1a and b). The island of Petite Terre was emplaced during the late stage of the volcanic activity in Mayotte. It is mostly made of pyroclastic rocks of phonolite/alkaline composition resulting from the crystal fractionation of magmas deriving from the partial melt of an oceanic lithosphere enriched in CO_2 (Pelleter *et al.*, 2014). The Dziani Dzaha is located in a volcanic crater formed by a phreatomagmatic eruption. The pyroclastic rocks rest over a coral reef dated from 9 ka, which surrounds the biggest island of Mayotte (*i.e.*, Grande Terre). The most recent volcanic event being dated at 4 ka (Zinke *et al.*, 2003), the age of the Dziani Dzaha may range from 9 ka to 4 ka.

The lake shows a roughly elliptical shape with a length of 640 meters and a width of 470 meters. The lake watershed is very restricted. The volcanic crater is ~1.2 km long from top to top, 50m high in average and the flanks consist of indurated layers of volcanic ashes and pumices. The lake bottom is approximately at sea level. It has an average depth of 3 meters and a maximal depth of 5 meters, except for a singular depression which downs to 18 meters (Fig. 1 and 2). This morphological feature is likely related to the phreatomagmatic eruption at the origin of the Dziani Dzaha. Magmatic degassing is still active in the island of Petite Terre, as evidenced by the four bubbling areas of

volcanic CO_2 identified at the lake surface. Microbialites, *i.e.*, organo-sedimentary structures formed in close association with microorganisms, thrive in the shallow waters of the lake and are mainly composed of aragonite and calcite (Gérard *et al.*, 2018). The distribution of the microbialites is patchy and mostly limited to the lake shore (Fig. 1) such that below a few tens of centimeters of water depth, most of the sediments are composed of gelatinous and non-indurated material.

The physical, chemical and biological features of the lake are very singular (Leboulanger *et al.*, 2017). The salinity of the lake water reaches up to 52 psu, *i.e.*, 1.5 times higher than seawater. The alkalinity is ~0.2 $mol \cdot L^{-1}$, with pH values ranging from 9.1 to 9.4. The mean daily surface temperature varies between 28 and 36°C. The lake ecosystem is massively dominated by prokaryotes with a dense and perennial bloom of filamentous cyanobacteria accounting for more than 90% of the primary producer biomass. The biologic activity is massive all year round, with a primary productivity of ~8 g of $C \cdot m^{-2} \cdot day^{-1}$, close to the maximum for tropical and subtropical lakes proposed by Lewis (2011).

3. Materials and methods

3.1. Nomenclature

The samples are named as follows. For DZ14-10 C4, "DZ" is for Dziani, "14-10" is for the year (2014) and the month (October) of the survey and C4 refers to the sediment core number 4 (see location in Figure 1). As the sediment cores were numbered according to their sampling order, they are named in Figure 1 and in the text only as C*X*, with *X* the number of the core from 1 to 13. Sediment cores C3, C5, C7, C8 and C12 were not dedicated to the study of the sediment composition and are not used in this study, except for the water content of sediment core C12. The samples are listed in Table A1 in supporting information.

3.2. Sampling, sample treatment and water content of sediment

Sediment cores were collected at different sites within the lake during the surveys performed in April 2012, April 2014, October 2014 and August 2016 (Table A1, Fig. 1). Data from 9 sediment cores are presented in this study: C1, C2, C4, C6, C9, C10, C11, C12 and C13. A Uwitec core sampler (90 mm in diameter PVC tubes) was used to collect sediment from the water-sediment interface to a maximum of one meter deep. The sediment cores were subsampled, as much as possible, on a color basis in the form of 3 to 5 cm thick slices, which were preserved under anoxic conditions in a cold room. The samples were freeze-dried, before being rinsed with deionized water, centrifuged 3 to 4 times, and crushed down to <80 µm. In the sediment core C12, the water content was estimated for 29 samples by weighting fresh samples before and after drying at 60°C. The precipitation of halite (NaCl) was corrected assuming salinity similar to that of the water column, *i.e.* of $52 g \cdot kg^{-1}$ (Leboulanger *et al.*, 2017). Given the number and size of sediment cores and their samplings during 4 different surveys

spread on a 4 year period, the analytical procedures presented below could not be performed on all samples.

3.3. Total carbon content and carbon isotope composition

The total carbon (TC) content and carbon isotope composition were analyzed on 101 samples of 7 sediment cores. The TC content was quantified with CHN elemental analyzer (Shimadzu TOC V CSH) on bulk samples with a precision of ±5wt.%. The isotopic composition of total carbon was analyzed with Flash-EA1112 elemental analyzer coupled to a Thermo Finnigan Delta^{plus} XP mass-spectrometer via a Conflo IV interface. Four organic laboratory standards were analyzed for concentration and isotopic calibration: VH1, CAP, MX33 and LC. Carbon isotopic compositions are reported relative to the Peedee belemnite (PDB) standard with a precision of ±0.5‰. In some samples, carbonates or organic matter were removed to measure the isotopic composition of the carbon endmembers. Decarbonatation was performed on 33 samples with HCl 6N and the carbon isotope composition of organic matter was measured by EA-IRMS. For 7 samples, organic matter was removed using low-temperature oxygen-plasma ashing in a POLARON PT7160 RF system and the carbon isotope composition of carbonates was measured with a Gas bench coupled to a Thermo Finnigan Delta^{plus} XP mass-spectrometer. Three laboratory carbonate standards were used for both carbonate quantification and for isotopic calibration: Across, Merck and Rennes II (details in Assayag *et al*, 2006; Lebeau *et al.*, 2014). Isotopic compositions are reported relative to the Peedee belemnite (PDB) standard for carbon with a precision of ±0.1‰. All carbonate and organic laboratory standards for C-isotope composition were calibrated independently against NBS19 and IAEA CO 1 international standards.

3.4. XRPD and XRF analyses

X-ray powder diffraction (XRPD) analyses were performed on 128 samples of 7 sediment cores and 12 samples of the volcanic catchment with an Empyrean (Panalytical) diffractometer equipped with a multichannel PIXcel 3D detector and a Cu Kα X-ray source (λ = 1.541874 Å). Each pattern was recorded in the θ-θ Bragg-Brentano geometry, in the 5°-90° 2θ range (0.0131° for 70 s). Analysis of X-ray patterns and mineralogical identification was performed using the High Score Plus software, the Crystallography Open Database (COD) and the Inorganic Crystal Structures Database (ISCD). The Reference Intensity Ratio (RIR) method was used for semi-quantifications of mineral phases; however, reference intensity ratios for clay minerals were frequently missing from the databases.

Elemental analyses were further conducted by Energy Dispersive X-ray fluorescence (EDXRF) on 99 samples of 6 sediment cores and 4 samples of the volcanic catchment with an epsilon 3XL (Panalytical) spectrometer equipped with a silver X-ray tube. A 10-minute measurement repeated 6 times for each sample yielded accurate quantitative analysis.

3.5. SEM and TEM analyses

Scanning and transmission electron microscopy were performed on crushed (<80µm) samples after freeze-drying and rinsing. Crushed samples were used for the microscope analyses because the preservation of textural relationships among different components was rendered difficult by the gelatinous texture of the sediment (see Section 4.1 below). Scanning Electron Microscopy (SEM) was performed on 19 samples with a Zeiss Ultra 55 FEG microscope operated at 10 kV and a working distance of 7.5 mm using mostly a backscattered electron detector for imaging. Transmission Electron Microscopy (TEM) was performed with a Jeol FEG 2100F operated at 200 kV on one clay-rich sample selected on the basis of the XRPD analyses. Both SEM and TEM were equipped with an energy dispersive X-ray system from Bruker and Jeol, respectively.

3.6. Clay fraction

Clay fraction analysis was performed on two clay-rich samples selected on the basis of the XRPD analyses of bulk samples. Carbonates were removed using the acetic acid-acetate buffer method (Ostrom, 1961). Organic matter was removed at 50°C by adding small aliquots of H_2O_2 to the suspension until gaseous emission had ceased. The <2 µm fraction was separated using gravity sedimentation of particles in water (Stoke's law), and then saturated with a 1 M NaCl solution for 24 h at room temperature. Oriented preparations of the Na-saturated <2 µm fraction were carried out on glass slides and dried at room temperature to obtain an air-dried (AD) preparation. Ethylene glycol (EG) solvation was achieved by exposing the oriented slides to ethylene glycol vapor for 12 h. Glycerol (GL) solvation was carried out by saturation of samples with a 2 M $MgCl_2$ solution for 24 h at room temperature and then exposure to glycerol vapor 3 days at 80°C. The air-dried oriented slide was also heated at 500°C for 90 minutes and then solvated in EG for 16h as described in details by Christidis and Koutsopoulou (2013). X-ray diffraction patterns were acquired on the oriented preparations over the 2–50 angular region, with 0.03° 2θ angular steps, using a Bruker D8 diffractometer equipped with Cu Kα radiation (λ = 1.5418 Å). Counting time was adapted to the low amount of sample available and is 1.65 s per step; the two Soller slits were 2.5°. Analysis of XRD patterns and mineralogical identification was performed using the Bruker Diffracplus EVA software and the ICDD database.

Electron microprobe analyses (EMPA) were conducted after coating of the < 2µm clay fraction with carbon. Spot analyses were performed using a CAMEBAX SX Five electron microprobe with an accelerating voltage of 15 kV, a beam current of 12 nA, and a 1 µm beam diameter. More details on the analytical methods are in Lerouge *et al.* (2017).

Cation Exchange Capacity (CEC) was measured using the hexamine cobalt(III) chloride method developed by Hadi *et al.* (2013) and adapted from Orsini and Remy (1976). The CEC is

deduced from two cross analyses: the amount of hexamine cobalt(III) that disappears from the solution (adsorbed on the clay), which is directly measured by spectrophotometry at 475 nm, and analysis by ionic chromatography (HPLC, Dionex) of the major cations present in the supernatant (Na^+, K^+, Ca^{2+}, Mg^{2+}) that also indicates the relative populations of desorbed exchangeable cations.

3.7. Quantification of sediment composition

On the basis of XRPD and XRF analyses, bulk carbon contents and carbon isotope compositions, calculation was performed to quantify the contents of the different mineral phases and of the organic matter. The organic matter content was calculated in two steps. First, the content of total organic carbon (TOC) is calculated using an isotope mass balance calculation. The total carbon content is a mixture between organic and inorganic carbon, for which the isotopic compositions were measured in this study. The contribution of organic carbon x in the total carbon content can hence be calculated with the equation:

$$\delta^{13}C_{TC} = x * \delta^{13}C_{TOC} + (1-x) * \delta^{13}C_{TIC} \quad (1)$$

with $\delta^{13}C$ of TC, TOC and TIC being the isotopic composition of total carbon, total organic carbon and total inorganic carbon, respectively. Then the TOC content is given by:

$$TOC = x * TC \quad (2)$$

Second, the content of organic matter was calculated considering a TOC to organic matter weight ratio of 1.9 (Broadbent, 1953). The mineral content is deduced by simple mass balance. For the sediment core C13, as the carbon content and the carbon isotope composition were not measured, the content of organic matter is considered to be the same as in C6, which is a reasonable assumption since the two cores were collected in the depression of the lake.

The content of each mineral phase was calculated using the XRF analyses, which requires fixing the chemical formula of each phase. Empirical formulas were used for most minerals (Table 1). For saponite, the structural formula has been determined in this study (Section 4.5). On the basis of SEM-EDS analyses of alkaline feldspars and volcanic pumices in lake sediment samples, the empirical formula of anorthoclase is considered for these phases. Then, the content of each mineral is calculated based on a given element.

3.8. Thermodynamic calculation

Mineral stability domains in the system Mg-Ca-C-O-H and Mg-Al-Si-O-H were calculated at 30°C and 1 bar with the Thermoddem database (Blanc et *al.*, 2012) and compared with lake water compositions (Leboulanger *et al.*, 2017). The speciation of dissolved species is calculated with the Phreeqc software (Parkhurst and Appelo, 2013).

4. Results

4.1. Description of lake sediment textures

Three main sediment textures have been observed within the lake (Fig. 2a). In the sediment cores collected at water depth ranging from 1 to 5 meters, which represents most of the lake area, the sediment texture is highly gelatinous and characterized by horizontal laminae (Fig. 2b). The uppermost sediment is markedly laminated with colors ranging from light to dark brown. The laminae are mostly <1 mm thick but seem to be organized, on a color basis, in laminae packages of few centimeters thick, which were used when possible to describe the slices cut from the sediment cores. In most case, grain size is indistinguishable to the eye, except in rare mudstone layers which contain grains of millimeter size. Below ~ 50 cm deep, the laminae tend to disappear and the sediment aspect changes to a more massive and darker texture. The water/rock weight ratio decreases from ~33 in surface sediments to ~4 at 20 cm deep and ~2 at one meter deep (Fig. 2d). Thus, water is by far the dominant phase of the sediment and most of the sediment compaction occurs in the first 20 cm below the sediment surface. This sedimentary facies is very homogeneous and no lateral variation has been observed in the area of 1 to 5 meter of water depth.

The sediment cores C12 and C13 collected in the depression of the lake show a similar sediment texture (highly gelatinous, laminated and with very fine grain size); however, deformation of the laminae is observed below ~30 cm deep (Fig. 2c). In the sediment cores close to the shoreline in shallow (<1 m) water depth (C9, C11), the sediment is grayish and grain size can increase up to the millimeter size. In C9, the sediment texture is close to that of a mudstone and remains relatively gelatinous and laminated. In C11, the sediment texture is close to a packstone and laminae are not visible. The thickness of the sediment column is unknown; however, attempts to collect longer sediment cores (C3, C4 and C5) in the area of 4 to 5 meters of water depth suggests that it is thicker than 2.3 m in this area.

4.2. Total carbon content and isotopic composition of the lake sediments

The content of total carbon decreases from ~ 35-40wt.% in the uppermost sediment to ~ 10-15wt.% at depth, except for the sediment cores collected in the depression of the lake (C6) and close to the shoreline (C9 and C11) (Table A2 in supporting information). In the depression of the lake (C6), the TC content ranges between 25 and 20wt.% and is relatively constant with depth. The TC content in C9 and C11 is lower with values of ~10wt.%. The sediment core C2 shows a local decrease of TC content down to 3wt.% at 7-14 cm deep.

The isotopic composition of total carbon is relatively constant with depth; however, the $\delta^{13}C$ values vary between ~ -15‰ and ~ +5‰ depending on the sediment core (Table A2). The highest

values are found in C11, whereas C1 and C2 show the lowest values. The variations of $\delta^{13}C$ values of total carbon between the sediment cores reflect variable proportions of organic and inorganic carbon. The isotopic compositions of the two carbon endmembers measured on samples of C6 and C9 are relatively constant with depth, with average $\delta^{13}C$ values of ~ -14‰ for organic carbon and ~ +16‰ for inorganic carbon (Table A2).

4.3. Chemical and mineralogical characterization of the sediment cores

4.3.1. Bulk analysis of the sediment cores (XRF)

The mineral content consists mostly of silicon, magnesium, calcium and aluminum (Table A3 in supporting information). Except for the sediment cores collected at the shoreline (C11) and in the lake depression (C6, C13), all sediment cores (*i.e.*, C4, C9 and C10) show a decrease of the magnesium content with depth and a concurrent increase of the aluminum and silicon contents, while the calcium content remains relatively stable. In the sediment core C11, the evolution of the chemical composition with depth is approximately the same, but the aluminum and silicon contents are higher than in C4, C9 and C10. In the sediment cores C6 and C13, the calcium, magnesium, aluminum and silicon contents are relatively stable with depth.

4.3.2. XRPD analyses of sediment cores

Aragonite, hydromagnesite and diopside or clinoenstatite, referred hereafter as clinopyroxene, are detected in the uppermost sediment (see Table A4 in supporting information). This mineral assemblage is relatively constant up to ~ 20 cm deep and occurs in all sediment cores collected under a water depth of >1m (*i.e.*, C2, C4, C6, C10, C13) . Semi-quantifications with the RIR method indicate contents of aragonite, hydromagnesite and clinopyroxene of 40wt.%, 40wt.% and 20wt.%, respectively. Minor phases such as magnetite, dolomite and quartz are sometimes identified with abundances of ~ 5-10wt.%. Halite is also occasionally detected but results from precipitation during freeze-drying. Some sediment cores present a peculiar assemblage: high amounts of alkaline feldspars in C11 close to the shoreline, calcite and alkaline feldspars between 7 and 14 cm deep in C2, magnesite in the uppermost sediment of C9 and pyrite and dolomite at depth.

In addition to the aragonite-hydromagnesite-clinopyroxene assemblage, clay minerals occur at depth, characterized by a diffraction peak close to 14.5 angstroms (Å), consistent with the basal spacing (001) of smectites, chlorite or vermiculite (Fig. 3) (the precise characterization of clay minerals is presented later in the paper). Overall, clays were detected in all sediment cores below ~10-15cm, except for the sediment cores collected at the shoreline (core C11 of only 30cm long) and in the depression of the lake (cores C6 and C13), in which clays may be absent or below XRD detection limit. Concurrent to the occurrence of clays, the content of hydromagnesite decreases with depth until

complete disappearance in the sediment cores sampled between 2 and 5 m of water depth (C2, C4, C9 and C10). In the other cores (C11, C6 and C13), the content of hydromagnesite remains relatively constant with depth.

4.3.3.Scanning and transmission electron microscopy

Observations with scanning electron microscope and chemical mapping show Mg-rich minerals forming platelets, typical of hydromagnesite, together with Ca-rich minerals corresponding to aragonite (Fig. 4a and b). Associated with the carbonates, a mineral phase rich in silicon, magnesium and aluminum is recognized (Fig. 4a, b and c). Observations with transmission electron microscope of minerals of similar chemical composition highlight the sheet structure of the phase (Fig. 4d and e). Significant amount of volcanic glass containing silicon, aluminum and lower amount of sodium and potassium, is also observed (Fig. 4f and g). The chemical composition is close to that of anorthoclase ($Na_{0.7}K_{0.3}AlSi_3O_8$) (Fig. 4h). This is consistent with the XRF and XRPD analysis of volcanic pumices and ash layers of the volcanic catchment (see Section A1, Figure A1, Table A5 and A6 in supporting information).

4.3.4.Characterization of the clay fraction

The <2 µm clay fraction was extracted from two samples: one from 27-30 cm deep in the sediment core C4 which corresponds to a layer rich in clays (Table A4); the other one from 67-72 cm deep in sediment core C6. The XRD patterns acquired on oriented slides are similar for the two samples. One may notice that although the clays were Na-saturated, the 001 reflection was at ~14.5 Å instead of 12.5 Å as expected for relative humidity condition normally occurring in the laboratory (Brindley and Brown, 1980, p. 204) (Fig. 5a and b). As this will be later on illustrated, CEC measurement carried out on this Na-saturated fraction indicates that the exchanger still contains a significant amount of magnesium, which therefore explains this value. The swelling of the (001) from 14.5 Å in the air-dried state towards 17 Å in the ethylene glycol state (Fig. 5b) indicates the presence of smectite or vermiculite (Brindley and Brown, 1980). Powder XRD indicates that the (060) peak position is 1.53 Å (Fig. 5a), which is characteristic of trioctahedral phyllosilicates (Moore and Reynolds, 1997). Based on EPMA analysis (*e.g.*, no Li and Zn that ruled out hectorite and sauconite, presence of Al that ruled out stevensite) and the fact that the phyllosilicate is trioctahedral, the remaining possibilities are saponite and vermiculite (Brindley and Brown, 1980, ch. 2, p. 172; Debure *et al.* 2016). Distinguishing between smectite or vermiculite is not an easy task. However, glycerol solvation on Mg-saturated samples, led to swelling with a basal reflection at 16.5 Å (Fig. 5c). This is consistent with the presence of saponite as vermiculite is not supposed to swell under these conditions (Walker, 1958; Brindley, 1966; Suquet *et al.*, 1975, Tosca *et al.*, 2011). The cation exchange capacity of ~87.1 meq/100g is also consistent with saponite, whereas values of approximately 120 meq/100g are reported for vermiculite

(Brindley and Brown, 1980, ch. 3, p. 204). In addition, the fact that the sample heated at 500°C still showed a 001 reflection expanding to 17.4 Å after ethylene glycol solvation (Fig. 5b) further supports the saponite hypothesis (Christidis and Koutsopoulou, 2013).

Cation population obtained from CEC measurement is consistent with EPMA (Table 2). The two methods led to similar Na^+ content, which is the main interlayer cation. Ca^{2+} and K^+ values are a bit higher by EPMA because part of K^+ present in the inner sphere complexes might be difficult to extract with the hexamine cobalt method (Hadi *et al.*, 2013). Mg content obtained by EPMA was ten times higher than the value obtain by CEC. The structural Mg content was deduced from the difference between EPMA and CEC measurements.

The mean structural formula was determined assuming that Al was preferentially tetrahedral, the rest being octahedral, and that Na, Ca and K were preferentially in the interlayers (Lerouge *et al.*, 2017). The calculation revealed that Fe was not in tetrahedral sites but in the octahedral ones. In order to equilibrate the charge, Fe was only in its ferric form (Fe^{3+}). Based on all those considerations, the mean structural formulae is $K_{0.01}Mg_{0.12}Ca_{0.02}Na_{0.28}(Mg_{2.22}Fe_{0.18}Al_{0.28}\square_{0.32})(Si_{3.61}Al_{0.39})O_{10}(OH)_2$ where □ is a vacant site. Due to its trioctahedral character, this formula is not in agreement with the clay mineralogy nomenclature defined by Guggenheim (2006) for saponite; however, it is consistent with literature data that reported vacancies (from 0.15 to 0.56 depending of the studies) in the octahedral position of ferric saponite (Post, 1984; Kodama *et al.*, 1988; Vincente *et al.*, 1996; Hicks *et al.*, 2014). In addition, the calculated charge per formula unit (0.57) is below 0.6 which is considered in the nomenclature as the boundary between saponite and vermiculite. The differences observed in the structural formula could be related to the occurrence of minor amounts of other clay minerals or minor non-clay impurities (amorphous and/or crystalline phases) in the samples that have not been identified. The terminology "saponite-like mineral" will be used in this paper to be consistent with the nomenclature and the characterization.

4.4. Quantification of the sediment content

Results of the calculation of the evolution of mineral composition and organic matter content with depth are shown in Figure 6 (Table A7 in supporting information). Apart for the sediment core C11, organic matter represents ~50wt.% of the uppermost sediment. In the sediment cores C4 and C10, hydromagnesite decreases with depth while the saponite-like mineral accumulates to reach up to 25wt.% at ~70 cm deep in C10. Concurrently, the content of organic matter decreases. The content of aragonite is relatively constant around 20wt.% whereas the proportion of primary silicates, dominated by alkaline feldspar, increases with depth to reach up to ~25wt.%. The sediment core C11 shows much higher amounts of alkaline feldspars than the others sediment cores, up to 50wt.%. Compared to C4 and C10, the sediment cores sampled in the depression of the lake (*i.e.*, C6 and C13) have lower

amounts of saponite-like mineral at depth and relatively stable contents of hydromagnesite and organic matter.

If correct, the calculation of mineral contents should fulfill an internal consistency. For instance, the sum of silicon content in alkaline feldspar and in the saponite-like mineral, which is calculated independently using the measured content of potassium and aluminum, respectively, should not exceed the total measured content of silicon. For the sediment cores C4, C10, C6 and C13, the calculated silicon content exceed by 10mol.% the measured silicon content for only ~10% of samples. These low errors validate the calculation for these sediment cores. In contrast, calculation for C9 is not shown due to a lack of internal consistency. The core C9 was collected close to the shoreline, where detrital influence is high. In this case, considering only alkaline feldspar and pyroxene as detrital inputs might be an oversimplification.

Sensitivity tests have been performed on several parameters including the TOC to organic matter weight ratio (± 0.1 unit), the empirical formula of clinopyroxene (enstatite or diopside), and the chemical composition of the saponite-like mineral (± 0.1 mol/mol of mineral on the Al, Si and Mg content). Most of these parameters modify by less than 10% the percentage content of each phase, except for aragonite (up to 20%).

4.5. Thermodynamic model

The chemical compositions of lake waters (Table A8 in supporting information) (Leboulanger *et al.*, 2017; Gerard *et al.*, 2018) are compared to the stability domains of carbonates and brucite in the system Mg-Ca-C-O-H (Fig. 7a). The pore waters are close to metastable equilibrium between aragonite and hydromagnesite, and supersaturated relative to dolomite.

The stability domains of Mg-silicates are represented in the system Mg-Al-Si-O-H, considering that aluminum behaves conservatively between the Al-bearing phases (Fig. 7b). Chlorites are not considered in the calculation as their formations are kinetically limited at ambient temperature and pressure (Meunier, 2005). High pH values together with high activities of Mg^{2+} and dissolved silica favor the stability of saponite compared to other aluminosilicates. The chemical composition of lake water is close to equilibrium with quartz and supersaturated relative to saponite, kerolite, talc and sepiolite.

5. Discussion

5.1. Sediment composition and distribution

Three main sedimentary facies were observed within the lake, which respond to a shore to basin central lake transect. Close to the shoreline, the grayish facies dominated by millimeter size grains is

relatively poor in organic matter and rich in primary silicates, alkaline feldspars and pyroxene, which highlights high detrital input from the volcanic catchment. In the 1 to 5 meter deep lake area, the gelatinous facies is dominated by organic matter and records low lateral variation. The detrital components decrease with distance to the lake shore. The laminated uppermost sediment is mostly formed of aragonite and hydromagnesite whereas, at depth, the sediment texture becomes massive and dark, and the hydromagnesite is replaced by the saponite-like mineral. The layers containing coarser grains and enriched in calcite and alkaline feldspar with less organic carbon (sediment core C2) reflects a local higher energy detrital input to the lake margin. In the central lake depression, the soft-sediment deformations are interpreted as slump events (Alsop and Marco, 2011). In this area, the apparently undeformed uppermost sediment is also rich in organic matter, aragonite and hydromagnesite but hydromagnesite persists at depth and the saponite-like mineral occurs in much lower amounts. No clay mineral has been detected in the uppermost part of sediment cores suggesting low amounts of detrital clays inherited from the weathering of the surrounding volcanic rocks.

Overall, the sediment deposited below 1 meter of water depth is singular by its extremely high content in organic matter (>50wt.%), a consequence of the intense primary productivity in the lake, and by the anomalously positive carbon isotope signature of both carbonates and organic matter, which probably resulted from a combination of volcanic CO_2 input and methanogenesis. The sediment collected between 1 and 5 meters of water depth is the most representative of the sedimentary deposits observed within the lake. It is used hereafter as a case study to develop a better understanding of the co-occurrences of carbonates and Mg-silicates.

5.2. Thermodynamic and kinetic controls on carbonates and saponite-like mineral formation

The lake water composition is close to equilibrium with aragonite and hydromagnesite and the presence of these two carbonates in the uppermost sediment indicates that they precipitate relatively rapidly from the lake water, either in the water column or at the sediment-water interface. The occurrence of aragonite is consistent with the Mg/Ca molar ratio >10 of the lake waters, which has been shown to favor the formation of aragonite rather than calcite (Simkiss, 1964; Taft, 1967; Debure *et al.*, 2013a and b; Zeyen *et al.*, 2017) Although thermodynamics suggests that magnesite and dolomite are the most stable Mg-bearing carbonates at surface temperature and pressure, kinetics exerts a strong primary control on their formation (*e.g.*, Sayles, 1973; Arvidson and MacKenzie, 1999; Gautier *et al.*, 2014), which may explain why they are only observed punctually.

Despite supersaturation of the lake water relative to saponite, kerolite, talc and sepiolite, none of these phases were detected in the mineral assemblage of the uppermost sediments, suggesting that they do not precipitate from the lake waters. Precipitation of Al-free Mg-silicates from lake waters is nonetheless possible, as exemplified by the magnesium depletion in Lake Turkana attributed to the precipitation of stevensite (Yuretich and Cerling, 1983; Cerling, 1996). Tosca (2015) proposed a

critical supersaturation allowing Al-free Mg-silicates to overcome kinetic barriers and to precipitate directly from the water column. In the Dziani Dzaha, the removal of magnesium by hydromagnesite precipitation likely hinders the achievement of this critical supersaturation, preventing the homogeneous nucleation of Al-free Mg-silicates in the water column. Regarding the Mg-aluminosilicates, they are expected to form mostly through heterogeneous nucleation (*e.g.*, Tosca, 2015; Tosca and Wright, 2015), because of the low solubility of aluminium in most cases and especially in alkaline lakes ($2.2\ 10^{-6}$ mol L^{-1} at pH 9). In this process, detrital Al-bearing silicates act as mineral precursors, lowering the supersaturation required for the formation of aluminosilicates. In the Dziani Dzaha, alkaline feldspars and volcanic glasses are the likely Al-bearing precursors, allowing the formation of the saponite-like mineral in the sediment.

Achievement of high pH values in the water column is one of the chief factors that enable supersaturation relative to saponite, aragonite and hydromagnesite. Consistently, Mg-silicates associated with carbonate sediments have been widely reported in alkaline lakes and evaporative basins of pH values > 9 (Van Denburgh, 1975; Yuretich and Cerling, 1983; Darragi and Tardy, 1987; Banfield *et al.*, 1991; Hay *et al.*, 1991; Hover *et al.*, 1999; Martini *et al.*, 2002; Bristow *et al.*, 2009). As for other alkaline and hypereuthrophic lakes (Lòpez-Archilla *et al.*, 2004), the intense primary productivity in the Dziani Dzaha is the most likely mechanism responsible for these pH values, according to the simplified reaction:

$$HCO_3^- + H_2O = \text{“}CH_2O\text{”} + OH^- + O_2 \qquad \text{R.1}$$

The development of this massive primary productivity could be linked to the input of volcanic CO_2 within the lake, which probably supplies primary productivity with carbon.

In addition to pH, magnesium and silica concentrations are critical for the formation of saponite. The magnesium concentration of ~4 mM is comparable to the ones of other alkaline lakes producing Mg-silicates (Van Denburgh, 1975; Yuretich and Cerling, 1983; Darragi and Tardy, 1987; Banfield *et al.*, 1991). However, due to the competition for magnesium between Mg-silicates and Mg-carbonates, silica might have a greater influence than magnesium on the formation of saponite (Zeyen *et al.*, 2017). The silica concentrations (~0.3 mM) are around two orders of magnitude higher than the usual concentration of surface oceans (<2 µM; Treguer *et al.*, 1995), where the efficiency of diatoms in precipitating silica drastically lowers the concentration (*e.g.*, Siever, 1992; Racki and Cordey, 2000). Because no spring inflows have been identified, these high silica concentrations are attributed to the weathering of volcanic terrains in a diatoms-poor lacustrine environment.

5.3. Early diagenetic formation of the saponite-like mineral

The evolution of the sediment composition with depth is the likely result of early diagenetic reactions. The appearance of the saponite-like mineral only at depth, in spite of its supersaturation in the lake water, can be explained by the intrinsic kinetics limit of saponite precipitation (*e.g.*, Tosca, 2015) and by the kinetics of dissolution of the Al-bearing detrital phase. The mineralization of organic matter is evidenced by the decrease of the TOC content with depth in all the cores. In the right proportions, the CO_2 produced by the mineralization of organic matter could account for a decrease of pH destabilizing hydromagnesite while allowing both aragonite and the saponite-like mineral to remain supersaturated. In addition, a genetic relationship may exist between hydromagnesite and the saponite-like mineral. Calculation of mineral stability domains (Fig. 7b) shows that the precipitation of saponite from supersaturated water tends to decrease the pH values, favoring the destabilization of hydromagnesite, which, in return, could supply with Mg the formation of saponite (Fig. 8). In addition to organic matter mineralization, CO_2-rich volcanic gases seeping from the volcanic basement could contribute to the pH decrease of pore waters.

Changes of palaeoenvironmental conditions throughout the lake history are less consistent than early diagenetic reactions to explain the evolution of the sediment composition. If the decreasing amount of hydromagnesite with depth was due to lower Mg concentrations in the palaeo-lake waters and/or lower pH values than currently observed, saponite supersaturation would also be lower, which is not compatible with the increasing amount of saponite-like mineral at depth. The diagenetic scenario is thus the most likely, even though it remains to be validated. This would require the assessment of the saturation state of pore waters and the quantitative evaluation, with reactive transport modeling, of the diagenetic reactions occurring in the sediment, including saponite precipitation, hydromagnesite destabilization and organic matter mineralization.

5.4. Implications for the formation and distribution of Mg-silicates of the South Atlantic rift basins

Mg-silicates (stevensite, kerolite and talc) have been identified in lacustrine Cretaceous carbonate reservoir rocks of the South Atlantic (Bertani and Carozzi, 1985a, 1985b; Rehim *et al.*, 1986; Wright, 2012; Tosca and Wright, 2015). Their formation was suggested to occur in lakes where volcanic terrains predominated (Cerling, 1994; Wright, 2012). However, the source of Si and Mg to account for the amount of Mg-silicate found in those rocks remains under discussion. Wright (2012) suggested that spring inflows, in addition to the weathering of volcanic terrains, might have been required to enable the formation of both carbonates and Mg-silicates.

The study case of the Dziani Dzaha suggests that high silica and magnesium concentrations can be reached in lakes throughout the weathering of volcanic alkaline terrains, without necessarily involving external inputs such as spring or hydrothermal inflows. The development of an intense

primary productivity, sustained both by the magmatic CO_2 and by the nutrients supplied by the volcanic terrains (such as iron, potassium and phosphorous), is most likely responsible for the high pH values. Thus, a genetic link may exist between volcanic alkaline terrains, organic-rich sediment and Mg-silicates. In the Doushantuo Formation (635-551 Ma), saponite is associated with TOC contents reaching up to 4wt.% (Bristow *et al.*, 2009). Using a carbon to organic matter ratio of 1.9 (Broadbent, 1953) and considering 66 wt.% loss of initial organic carbon by thermal maturation (Tissot and Welte, 1984), the initial content of organic matter in the Doushantuo sediments may have been of ~23wt.%, which is comparable to the Dziani Dzaha sediments. The deposition of lacustrine carbonates containing more than 20wt.% of organic matter could have required a significant source of carbon in addition to the atmospheric CO_2. In the Dziani Dzaha, the volcanic CO_2 may have played a major role by fueling both the primary productivity and the carbonate factory. Similarly, the Cretaceous lakes at the origin of the South Atlantic carbonate reservoir rocks could have been influenced by CO_2-rich magmatic inflows during the continental rifting, as the continental crust becomes thinner and the influence of mantle fluids increases.

The absence of Al-free Mg-silicates in the Dziani Dzaha sediment, whereas they prevail in the carbonate reservoirs of the South Atlantic, supports two mutually compatible hypotheses as to the factors controlling the presence or absence of Al in Mg-silicates. At the local scale, this supports the "clay-zoning" scenario of Millot *et al.* (1970), who suggested that the presence of detrital Al-bearing silicates at the basin margin allows Al-rich clay minerals to form, whereas, toward the basin center, lower amounts of detrital materials indirectly promote the homogeneous nucleation of Al-free Mg-silicates (Weaver and Beck, 1977; Jones and Weir, 1983; Jones, 1986; Calvo *et al.*, 1999; Deocampo *et al.*, 2009; Galán and Pozo, 2011). Accordingly, the occurrence of a saponite-like mineral in the Dziani Dzaha is consistent with the presence of detrital component in the sediments and the prevalence of Al-free Mg-silicates in the South Atlantic carbonate reservoirs would rather indicate large lake systems with open water lake deposits free from detrital inputs.

At the regional scale, the formation of saponite or Al-free Mg-silicates may also reflect the nature of the volcanic terrains hosting the lacustrine environments. At the early stage of continental rifting, low mantle uplift results in low partial melting, producing alkaline magma (*e.g.*, White and McKenzie, 1989; Wilson, 1992). Below the thick continental lithosphere, the slow cooling of magmas generates highly differentiated basalts enriched in alkaline elements, aluminum and silicon, *i.e.*, a phonolite/alkaline composition comparable to the one of magmas at the origin of the Mayotte Islands. In contrast, during later stages of continental rifts, higher partial melting and lower magmatic differentiation produce tholeiitic basalts with lower aluminum content. The relatively low availability of aluminum in the Cretaceous lakes at the origin of the South Atlantic carbonate reservoirs may indicate lacustrine environments formed during the late stage of continental rifting. This is consistent with the suggestion of Tosca and Wright (2015) that the water chemistry of these lakes may have been

influenced by the serpentinization of exhumed mantle at the transition between continental and oceanic crusts.

6. Concluding remarks

The Dziani Dzaha sediment exhibits a particular evolution of composition in the first meter of sediment, which can be explained by early diagenetic reactions within the lake sediments. These are mainly gelatinous and exhibit homogeneous facies distribution with local increases in detrital inputs close to the shore. Mineralization of organic matter within the sediment, possibly associated with inputs of volcanic CO_2, can explain the destabilization of hydromagnesite and the decrease of organic matter content with depth, while aragonite remains stable. Kinetic limitation prevents the formation of the saponite-like mineral in the uppermost sediment, such that it only accumulates below 15 cm depth. Reactive transport modeling is now needed to allow a quantitative evaluation of the role of all diagenetic processes occurring in these sediments: saponite precipitation, hydromagnesite destabilization, organic matter mineralization and/or CO_2-rich gas inputs.

The formation of the saponite-like mineral in the Dziani Dzaha results from the high silica activities and the high pH values of the lake waters. This water chemistry is attributed to the delivery in a restricted lake system of chemical elements, among which nutrients, produced by the weathering of volcanic terrains, which favors the development of an intense primary productivity. The bubbling of magmatic gases in the Dzaini Dzaha suggests that magmatic CO_2 may fuel the primary productivity and the carbonate precipitation. Thus, our study suggests that a genetic link may exist between volcanic contexts and carbonate sediments rich in organic matter and Mg-silicates, which may be key in understanding their formation throughout the fossil record. As an example, the migration through the crust of mantle-derived fluids during continental rifting could have influenced the formation of the Cretaceous South Atlantic carbonate reservoir rocks. In these rocks, the formation of Al-free Mg-silicates rather than saponite may be indicative of low aluminum availability, favored in large lacustrine environments hosted in poorly differentiated volcanic terrains commonly emplaced during late stages of continental rifting.

ACKNOWLEDGMENT

This work was supported by IPGP, TOTAL (project FR00008189), Agence Nationale de la Recherche (France) (ANR DZIANI, grant number ANR-13-BS06-0001), Total Corporate Foundation (project 755 DZAHA) and one INSU-INTERRVIE grant (grant number AO2013-785992). The Deep Carbon Observatory community is thanked here for several informative discussions on the importance of studying environments related to magmatic CO_2 emissions. The authors also wish to thank their colleagues (C. Leboulanger, C. Bernard, P. Got, E. Fouilland, M. Bouvy, E. Le Floch, V. Grossi and D. Sala) for their support and assistance during sampling campaigns on Dziani Dzaha. Last but not least, they thank the Air Austral Airline Company and Alexandra and Laurent at the "Les Couleurs" Guest House in Mayotte for their valuable assistance and support.

REFERENCES

Alsop G.I. and Marco S. (2011) Soft-sediment deformation within seismogenic slumps of the Dead Sea Basin. *Journal of Structural Geology*, **33**(4), 433-457.

Arvidson R.S. and Mackenzie F.T. (1999) The dolomite problem; control of precipitation kinetics by temperature and saturation state. *American Journal of Science*, **299**(4), 257-288.

Assayag N., Rivé K., Ader M., Jézéquel D. and Agrinier P. (2006) Improved method for isotopic and quantitative analysis of dissolved inorganic carbon in natural water samples. *Rapid Communications in Mass Spectrometry*, **20**(15), 2243-2251.

Banfield J.F., Jones B.F. and Veblen D.R. (1991) An AEM-TEM study of weathering and diagenesis, Abert Lake, Oregon, II. Diagenetic modification of the sedimentary assemblage. *Geochimica and Cosmochimica Acta*, **55**, 2795–2810.

Bertil D. and Regnoult J.M. (1998) Seismotectonic of Madagascar. *Tectonophysics*, **294**, 57-74.

Bertani R.T. and Carozzi A.V. (1985) Lagoa feia formation (Lower Cretaceous), Campos basin, offshore Brazil: rift valley stage lacustrine carbonate reservoirs-I. *Journal of Petroleum Geology*, **8**(1), 37-58.

Bertani R.T. and Carozzi A.V. (1985) Lagoa feia formation (Lower Cretaceous), Campos basin, offshore Brazil: rift valley type lacustrine carbonate reservoirs-II. *Journal of Petroleum Geology*, **8**(2), 199-220.

Blanc P., Lassin A., Piantone P., Azaroual M., Jacquemet N., Fabbri A. and Gaucher E. C. (2012) Thermoddem: A geochemical database focused on low temperature water/rock interactions and waste materials. *Applied Geochemistry*, **27**(10), 2107-2116.

Brindley G.W. (1966) Ethylene Glycol and Glycerol Complexes of Smectites and Vermiculites. *Clay Minerals* **6**, 237-259.

Brindley G.W. and Brown G. (1980) Crystal structures of clay minerals and their X-Ray identification. *Mineralogical Society Monograph* **5**, London.

Bristow T.F., Kennedy M.J., Derkowski A., Droser M.L., Jiang G.Q. and Creaser R.A. (2009) Mineralogical constraints on the palaeoenvironments of the Ediacaran Doushantuo Formation. *Proceedings of the National Academy of Sciences of the USA*, **106**, 13190–13195.

Broadbent F.E. (1953) The soil organic fraction. *Advances in agronomy*, **5**, 153-183.

Calvo J.P., Blanc-Valleron M.M., Rodriguez-Arandia J.P., Rouchy J.M. and Sanz M.E. (1999) Authigenic clay minerals in continental evaporitic environments. In: Thiry M. and Simon-Coinçon R. (eds) Palaeoweathering, Palaeosurfaces and Related Continental Deposits. International Association of Sedimentologists, Special Publications, **27**, 129–151.

Cerling T.E. (1996) Pore water chemistry of an alkaline lake: Lake Turkana, Kenya. In: Johnson, T. C. & Odada, E. O. (eds) Limnology, Climatology and Paleoclimatology of the East African Lakes. Gordon and Breach, Amsterdam, 225–240.

Chamley H. (1989) *Clay Sedimentology* (Springer, Berlin).

Christidis G.E. and Koutsopoulou E. (2013) A simple approach to the identification of trioctahedral smectites by X-ray diffraction. *Clay Minerals*, **48**(5), 687-696.

Coltorti M., Bonadiman C., Hinton R.W., Siena F. and Upton B.G.J. (1999) Carbonatite metasomatism of the oceanic upper mantle: evidence from clinopyroxenes and glasses in ultramafic xenoliths of Grande Comore, Indian Ocean. *Journal of Petrology*, **40**, 133-165.

Darragi F. and Tardy Y. (1987) Authigenic trioctahedral smectites controlling pH, alkalinity, silica and magnesium concentrations in alkaline lakes. *Chemical Geology*, **63,** 59–72.

Debure M., De Windt L., Frugier P., Gin S. and Vieillard P. (2016) Mineralogy and thermodynamic properties of magnesium phyllosilicates formed during the alteration of a simplified nuclear glass. *Journal of Nuclear Materials*, **475**, 255-265.

Debure M., De Windt L., Frugier P. and Gin S. (2013a) HLW glass dissolution in the presence of magnesium carbonate: Diffusion cell experiment and coupled modeling of diffusion and geochemical interactions. *Journal of Nuclear Materials*, **443**(1), 507-521.

Debure M., Frugier P., De Windt L. and Gin S. (2013b) Dolomite effect on borosilicate glass alteration. *Applied geochemistry*, **33**, 237-251.

Deocampo D.M., Cuadros J., Wing-Dudek T., Olives J. and Amouric M. (2009) Saline lake diagenesis as revealed by coupled mineralogy and geochemistry of multiple ultrafine clay phases: Pliocene Olduvai Gorge, Tanzania. *American Journal of Science*, 309, 834–858.

Galán E. and Pozo M. (2011) Palygorskite and sepiolite deposits in continental environments. Description, genetic patterns and sedimentary settings. In: Galán E. and Singer A. (eds) Developments in Palygorskite–Sepiolite Research. Developments in Clay Science, 3. Elsevier, Amsterdam, 125–173.

Gautier Q., Bénézeth P., Mavromatis V. and Schott J. (2014) Hydromagnesite solubility product and growth kinetics in aqueous solution from 25 to 75°C. Geochimica et Cosmochimica Acta, 138, 1-20.

Gérard E., De Goeyse S., Hugoni M., Agogue H., Richard L., Milesi V., Guyot F., Lecourt L., Borensztajn S., Leclerc T., Joseph M., Sarazin G., Jezequel D., Leboulanger C. and Ader M. (2018) Key role of Alphaproteobacteria and Cyanobacteria in the formation of stromatolites of Lake Dziani Dzaha (Mayotte, Western Indian Ocean). *Front. Microbiol.* **9**, 796.

Guggenheim S., Adams J. M., Bain D. C., Bergaya F., Brigatti M. F., Drits V. A., Formoso Mr LL, Galán E., Kogure T. and Stanjek H. (2006). Summary of recommendations of nomenclature committees relevant to clay mineralogy: report of the Association Internationale pour l'Etude des Argiles (AIPEA) Nomenclature Committee for 2006. *Clay Minerals*, **41**(4), 863-877.

Hadi J., Tournassat C., Ignatiadis I., Greneche J. M. and Charlet L. (2013) Modelling CEC variations versus structural iron reduction levels in dioctahedral smectites. Existing approaches, new data and model refinements. *Journal of colloid and interface science*, **407**, 397-409.

Hay R.L., Guldman S.G., Matthews J.C., Lander R.H., Duffin M.E. and Kyser T.K. (1991) Clay mineral diagenesis in core KM-3 of Searles Lake, California. *Clays and Clay Minerals*, **39**(1), 84-96.

Hicks L.J., Bridges J.C. and Gurman S.J. (2014) Ferric saponite and serpentine in the nakhlite martian meteorites. *Geochim. Cosmochim. Ac.*, **136**, 194-210.

Hover V.C., Walter L.M., Peacor D.R. and Martini A.M. (1999) Mg-smectite authigenesis in a marine evaporative environment, Salina Ometepec, Baja California. *Clays and Clay Minerals*, **47**, 252–268.

Huang J., Chu X., Lyons T. W., Planavsky N. J. and Wen H. (2013) A new look at saponite formation and its implications for early animal records in the Ediacaran of South China. *Geobiology*, **11**(1), 3-14.

Jones B.F. (1986) Clay mineral diagenesis in lacustrine sediments. In: Mumpton, F. A. (ed.) Studies in Diagenesis. United States Geological Survey, Bulletin, **1578**, 291–300.

Jones B.F. and Weir A.H. (1983) Clay minerals of Lake Abert, an alkaline, saline lake. *Clays and Clay Minerals*, **31**, 161-172.

Kodama H., De Kimpe C.R. and Dejou J. (1988) Ferrian saponite in a gabbro saprolite at Mont Mégantic, Quebec. *Clays Clay Miner.*, 36(2), 102-110.

Lebeau O., Busigny V., Chaduteau C. and Ader M. (2014) Organic matter removal for the analysis of carbon and oxygen isotope compositions of siderite. *Chemical Geology*, **372**, 54-61.

Leboulanger C., Agogué H., Bernard C., Bouvy M., Carré C., Cellamare M., *et al.* (2017) Microbial Diversity and Cyanobacterial Production in Dziani Dzaha Crater Lake, a Unique Tropical Thalassohaline Environment. *PLoS ONE* **12**(1): e0168879.

Lerouge C., Gaboreau S., Grangeon S., Claret F., Warmont F., Jenni A., Cloet V. and Mäder U. (2017) In situ interactions between Opalinus Clay and Low Alkali Concrete, *Physics and Chemistry of the Earth*, **99**, 3-21.

Lewis Jr, W.M. (2011) Global primary production of lakes: 19th Baldi Memorial Lecture. *Inland Waters*, **1**(1), 1-28.

Lòpez-Archilla A.I., Moreira D., López-García P. and Guerrero C. (2004) Phytoplankton diversity and cyanobacterial dominance in a hypereutrophic shallow lake with biologically produced alkaline pH. *Extremophiles*, **8**(2), 109-115.

Martini A.M., Walter L.M., Lyons T.W., Hover V.C. and Hansen J. (2002) Significance of earlydiagenetic water-rock interactions in a modern marine siliciclastic/evaporite environment: Salina Ometepec, Baja California. *Geol. Soc. Am. Bull.* **114**, 1055–1069.

Meunier A. (2005) in *Clays*. (Springer, Berlin).

Millot G. (1970) in Geology of clays (*Springer-Verlag*).

Mougenot D., Hernandez J. and Virlogeux P. (1989) Structure et volcanisme d'un rift sous-marin; le fosse des Kerimbas (marge nord-mozambique). Bulletin de la Société Géologique de France, (2), 401-410.

Moore D.M. and Reynolds R.C. (1989) X-ray Diffraction and the Identification and Analysis of Clay Minerals (Vol. 332). New York: Oxford university press.

Nougier J., Cantagrel J.M. and Karche J.P. (1986) The Comores archipelago in the western Indian Ocean: volcanology, geochronology and geodynamic setting. *Journal of African Earth Sciences*, **5**, 135-145.

Orsini L. and Remy J.C. (1976) Utilisation du chlorure de cobaltihexamine pour la détermination simultanée de la capacité d'échange et des bases échangeables des sols. *Sci. Sol*, **4**, 269-275.

Ostrom M.E. (1961) Separation of clay minerals from carbonate rocks by using acid. *Journal of Sedimentary Research*, **31**(1).

Pace A., Bourillot R., Bouton A., Vennin E., Galaup S., Bundeleva I., Patrier P., Dupraz C., Thomazo C., Sansjofre P., Yokoyama Y., Franceschi M., Anguy Y., Pigot L., Virgone A. and Visscher P.T. (2016) Microbial and diagenetic steps leading to the mineralisation of Great Salt Lake microbialites. *Scientific reports*, **6**.

Parkhurst D.L. and Appelo C.A.J. (2013) Description of input and examples for PHREEQC version 3: a computer program for speciation, batch-reaction, one-dimensional transport, and inverse geochemical calculations (No. 6-A43). US Geological Survey.

Pelleter A.A, Caro M., Cordier C., Bachélery P., Nehlig P., Debeuf D. and Arnaud N. (2014) Melilite-bearing lavas in Mayotte (France): An insight into the mantle source below the Comores. *Lithos*, **208-209**, 281-297.

Post J.L. (1984) Saponite from near Ballarat, California. *Clays Clay Miner.*, 32(2), 147.

Racki G. and Cordey F. (2000) Radiolarian palaeoecology and radiolarites: is the present the key to the past? *Earth-Science Reviews*, **52**(1), 83-120.

Rehim H., Mizusaki A.M.P., Carvalho M.D. and Monteiro M. (1986) Talco e estevensita na formação lagoa feia da bacia de campos--possíveis implicações no ambiente deposicional. In: SBG, congresso brasileiro de geologia, 34, 416-425.

Sayles F L. and Fyfe W.S. (1973) The crystallization of magnesite from aqueous solution. *Geochimica et Cosmochimica Acta*, **37**(1), 87-96.

Setti M., Marinoni L. and Lopez-Galindo A. (2004) Mineralogical and geochemical characteristics (major, minor, trace elements and REE) of detrital and authigenic clay minerals in a Cenozoic sequence from Ross Sea, Antarctica. *Clay Minerals*, **39**, 405–421.

Siever R. (1992) The silica cycle in the Precambrian. *Geochimica et Cosmochimica Acta*, **56**(8), 3265-3272.

Simkiss K. (1964) Variation of the crystallization form of calcium carbonate from artififial sea water. *Nature*, **201**, 492-493.

Stoessell R. K. (1988) 25°C and 1 atm dissolution experiments of sepiolite and kerolite. *Geochim. et Cosmochim. Ac.* **52**(2), 365-374.

Suquet H., de la Calle C. and Pezerat H. (1975) Swelling and Structural Organization of Saponite. *Clays and Clay Minerals* **23**, 1-9.

Taft W.H. (1967) Physical chemistry of formation of carbonates. Elsevier, Amsterdam.

Tissot B.P. and Welte D.H. (1984) Diagenesis, catagenesis and metagenesis of organic matter. In Petroleum Formation and Occurrence (pp. 69-73). Springer Berlin Heidelberg.

Tosca N.J. (2015) Geochemical pathways to Mg-clay formation. In: Pozo M. and Galán E. (eds) Magnesian Clays: Characterization, Origins and Applications. AIPEA (Association Internationale pour l'Etude des Argiles), Special Publications, **2**, 283–329.

Tosca N.J., Macdonald F.A., Strauss J.V., Johnston D.T. and Knoll A.H. (2011) Sedimentary talc in Neoproterozoic carbonate successions. *Earth and Planetary Science Letters*, **306**(1-2), 11-22.

Tosca N.J. and Wright V.P. (2015) Diagenetic pathways linked to labile Mg-clays in lacustrine carbonate reservoirs: a model for the origin of secondary porosity in the Cretaceous pre-salt Barra Velha Formation, offshore Brazil. Geological Society, London, Special Publications, 435, SP435-1.

Treguer P., Nelson D.M., Van Bennekom A.J., DeMaster D.J., Leynaert A. and Quéguiner B. (1995) The silica balance in the world ocean: a reestimate. *SCIENCE-NEW YORK THEN WASHINGTON*, 375-375.

Van Denburgh A.S. (1975) in: Solute Balance at Abert and Summer Lake, South-central Oregon. (US Geological Survey, Washington), Professional paper 502-C.

Vicente M.A., Suárez M., López-González J.D.D. and Banares-Munoz M.A. (1996) Characterization, surface area, and porosity analyses of the solids obtained by acid leaching of a saponite. *Langmuir*, **12**(2), 566-572.

Walker G.F. (1958) Reactions of expanding-lattice clay minerals with glycerol and ethylene glycol. *Clay Minerals Bulletin*, **3**, 302-313.

Weaver C.E. (1989) *Clays, Muds, and Shales* (Elsevier, Amsterdam).

Weaver C.E. and Beck K.C. (1977) Miocene of the S.E. United States: A model for chemical sedimentation in a peri-marine environment. *Sedimentary Geology*, **17**, 1-234.

White R. and McKenzie D. (1989) Magmatism at rift zones: the generation of volcanic continental margins and flood basalts. *Journal of Geophysical Research: Solid Earth*, **94**(B6), 7685-7729.

Wilson M. (1992) Magmatism and continental rifting during the opening of the South Atlantic Ocean: a consequence of Lower Cretaceous super-plume activity? Geological Society, London, Special Publications, **68**(1), 241-255.

Wright V.P. (2012) Lacustrine carbonates in rift settings: the interaction of volcanic and microbial processes on carbonate deposition. Geological Society, London, Special Publications, **370**(1), 39-47.

Wright V.P. and Barnett A. (2015) An abiotic model for the development of textures in some South Atlantic early Cretaceous lacustrine carbonates. In: Bosence D.W.J., Gibbons K.A., Le Heron D.P., Morgan W.A., Pritchard T. and Vining B.A. (eds) Microbial Carbonates in Space and Time: Implications for Global Exploration and Production. Geological Society, London, Special Publications, 418, 209–219.

Yuretich R.F. and Cerling T.E. (1983) Hydrogeochemistry of Lake Turkana, Kenya: Mass balance and mineral reactions in an alkaline lake. *Geochimica and Cosmochimica Acta*, **47**, 1099–1109.

Zeyen N., Benzerara K., Li J., Groleau A., Balan E., Estève I., Tavera R., Moreira D. and López-García P. (2015) Formation of low-T hydrated silicates in modern microbialites from Mexico and implications for microbial fossilization. *Frontiers in Earth Science*, **3**, 64.

Zeyen N., Daval D., Lopez-Garcia P., Moreira D., Gaillardet J. and Benzerara K. (2017) Geochemical Conditions Allowing the Formation of Modern Lacustrine Microbialites. *Procedia Earth and Planetary Science*, **17**, 380-383.

Zinke J., Reijmer J.J.G. and Thomassin B.A. (2003) Systems tracts sedimentology in the lagoon of Mayotte associated with the Holocene transgression. *Sedimentary Geology*, **160**, 57-784.

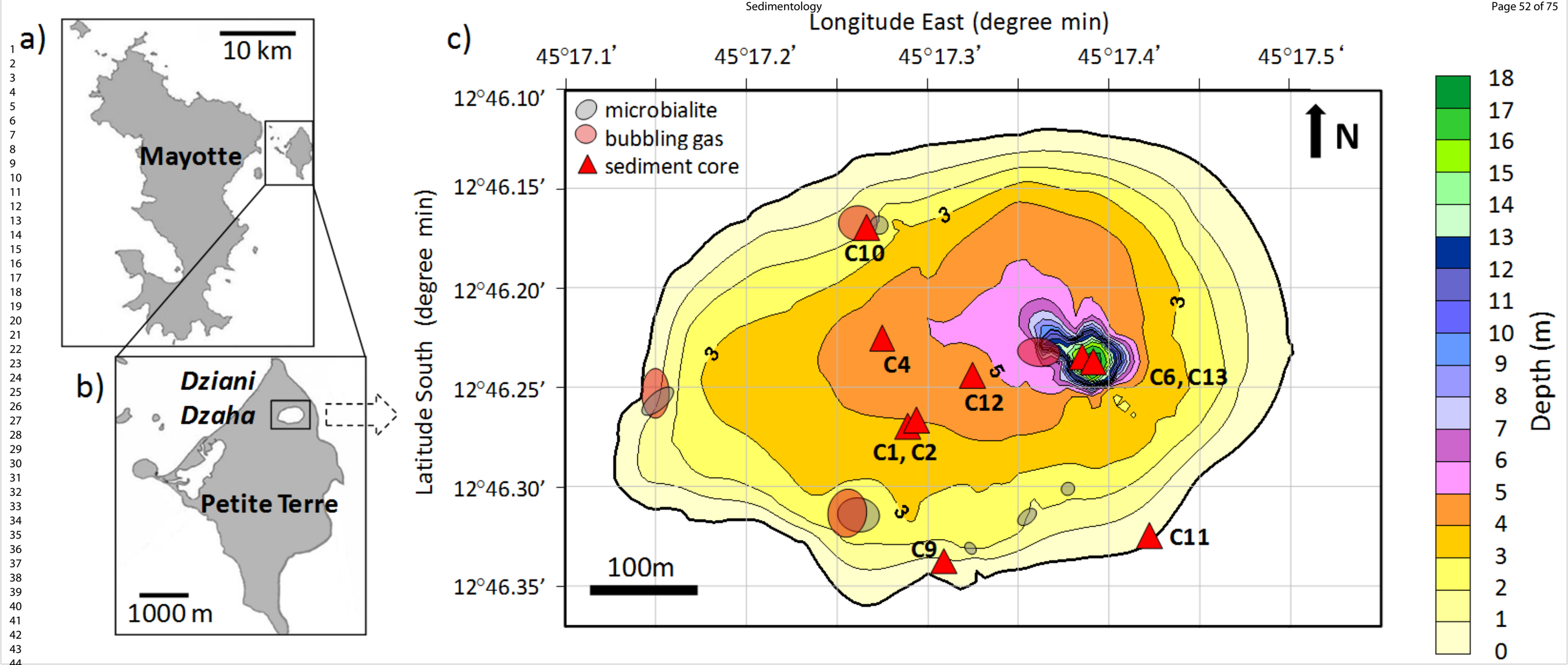
a)
10 km
Mayotte
b)
Dziani
Dzaha
Petite Terre
1000 m
c)
Longitude East (degree min)
45°17.1'
45°17.2'
45°17.3'
45°17.4'
45°17.5'
Latitude South (degree min)
12°46.10'
12°46.15'
12°46.20'
12°46.25'
12°46.30'
12°46.35'
microbialite
bubbling gas
sediment core
N
C10
C4
C12
C1, C2
C9
C11
C6, C13
3
5
100m
Depth (m)
0
1
2
3
4
5
6
7
8
9
10
11
12
13
14
15
16
17
18

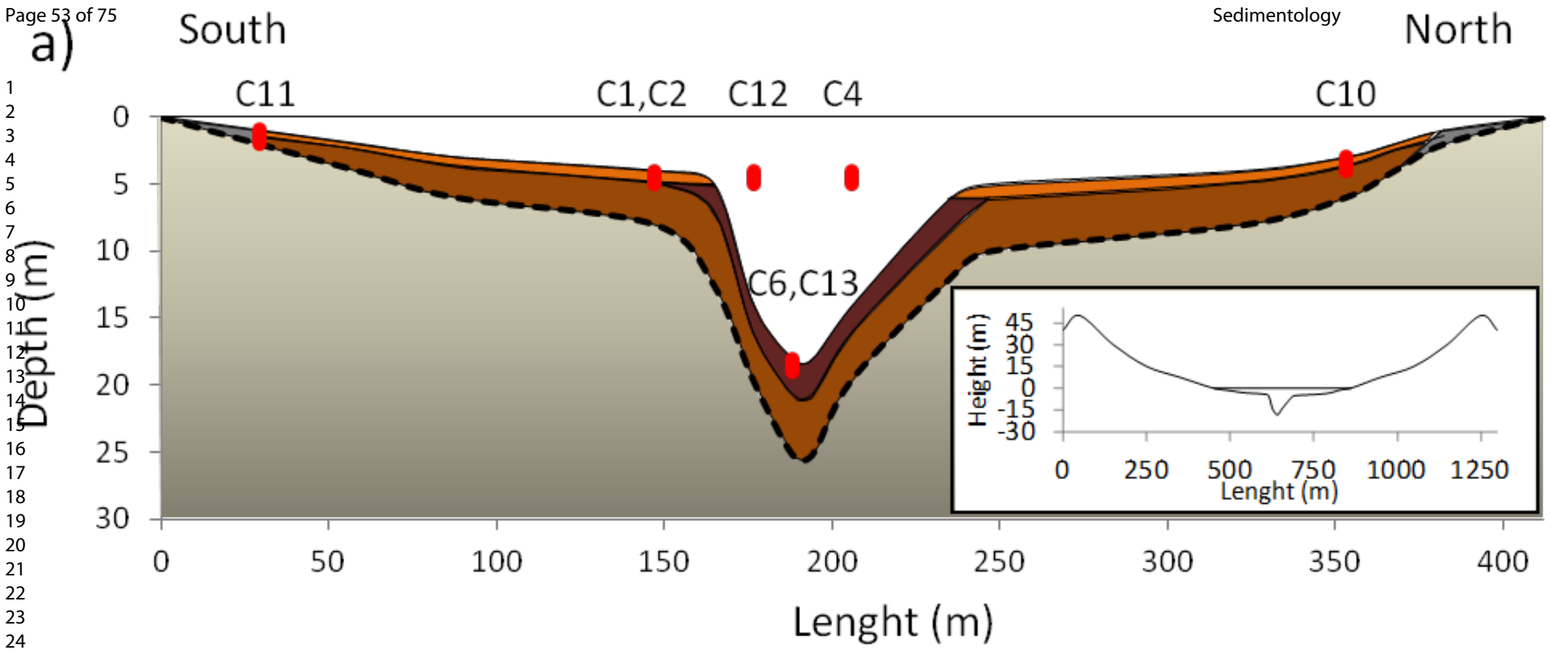
a)
South
North
C11
C1,C2
C12
C4
C10
C6,C13
Depth (m)
0
5
10
15
20
25
30
0
50
100
150
200
250
300
350
400
Lenght (m)
Height (m)
45
30
15
0
-15
-30
0
250
500
750
1000
1250
Lenght (m)

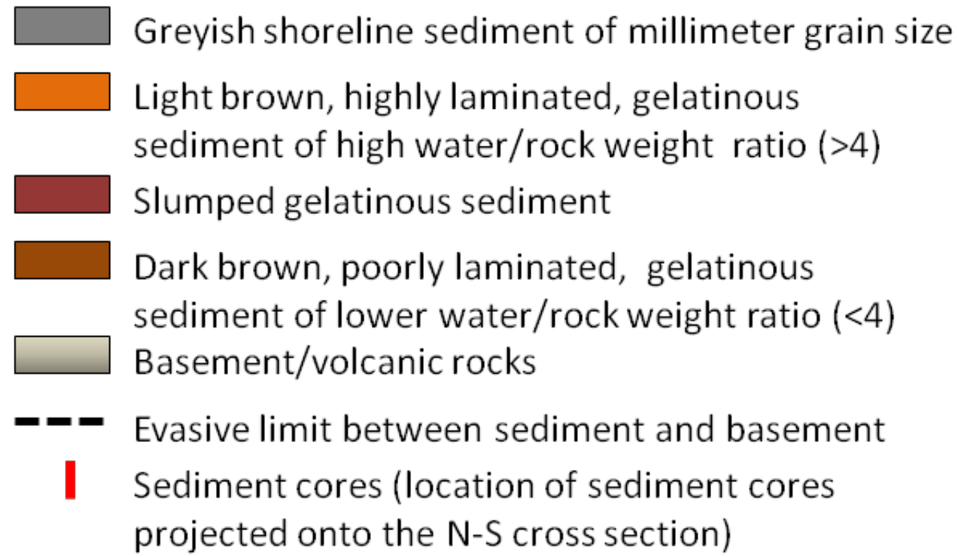
Greyish shoreline sediment of millimeter grain size
Light brown, highly laminated, gelatinous sediment of high water/rock weight ratio (>4)
Slumped gelatinous sediment
Dark brown, poorly laminated, gelatinous sediment of lower water/rock weight ratio (<4)
Basement/volcanic rocks
Evasive limit between sediment and basement
Sediment cores (location of sediment cores projected onto the N-S cross section)

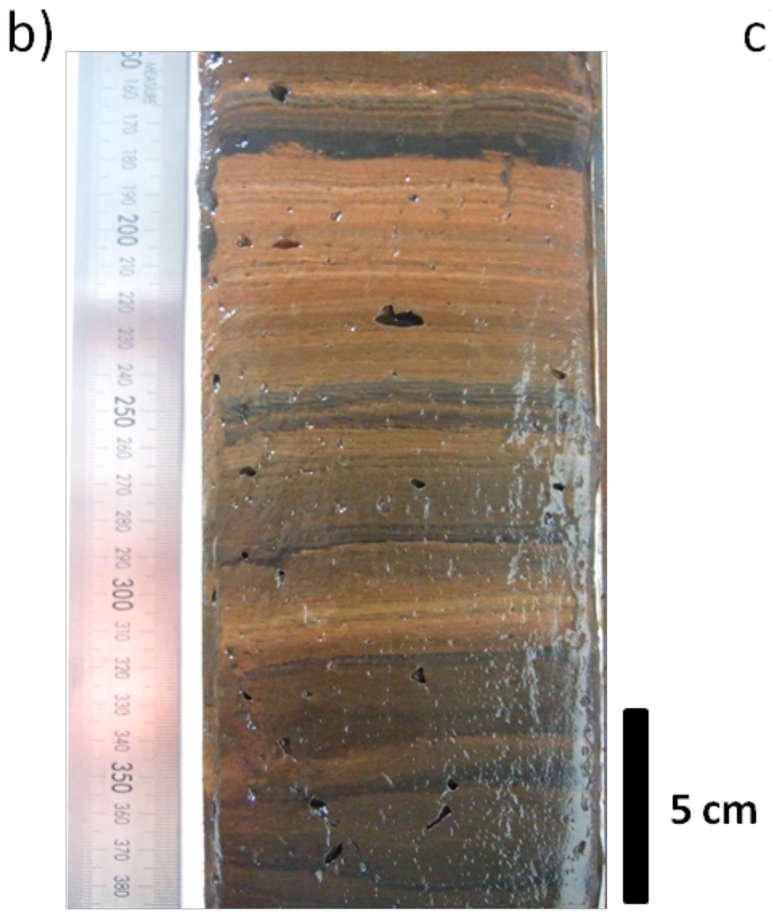
b)
5 cm

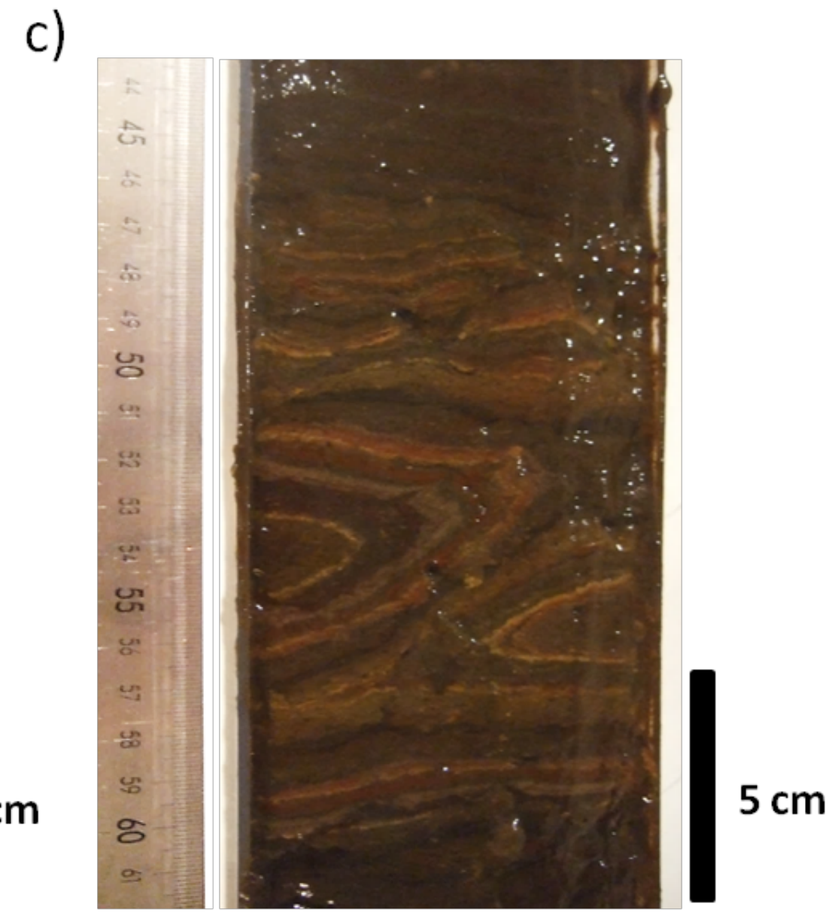
c)
5 cm

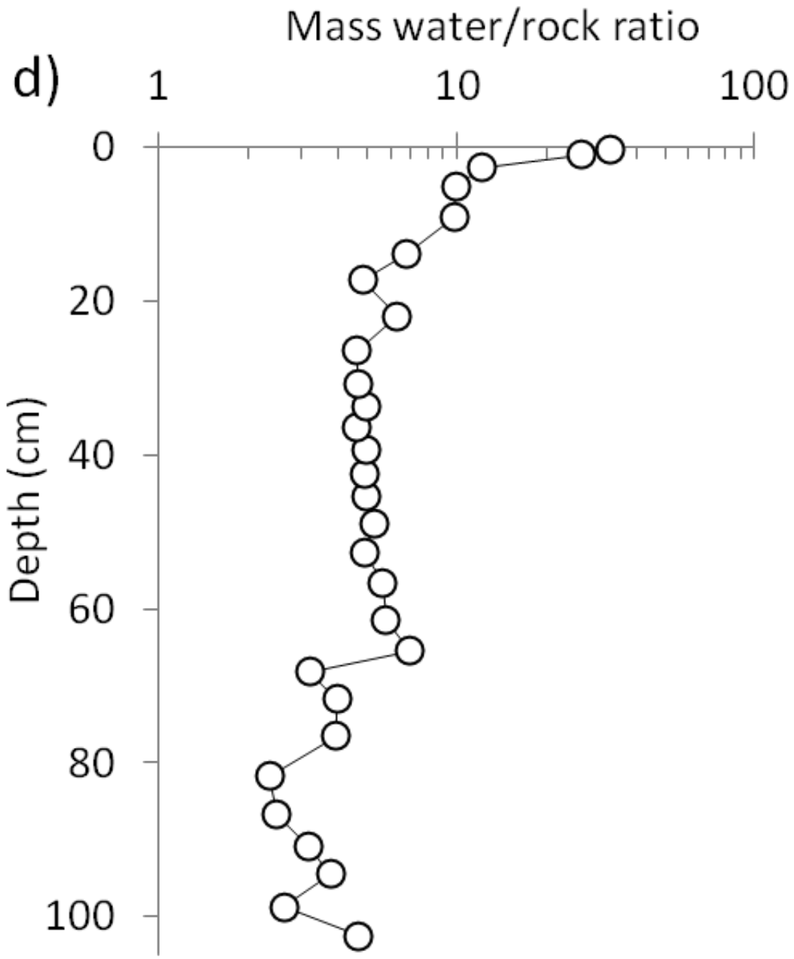
d)
Mass water/rock ratio
1
10
100
0
20
40
60
80
100
Depth (cm)

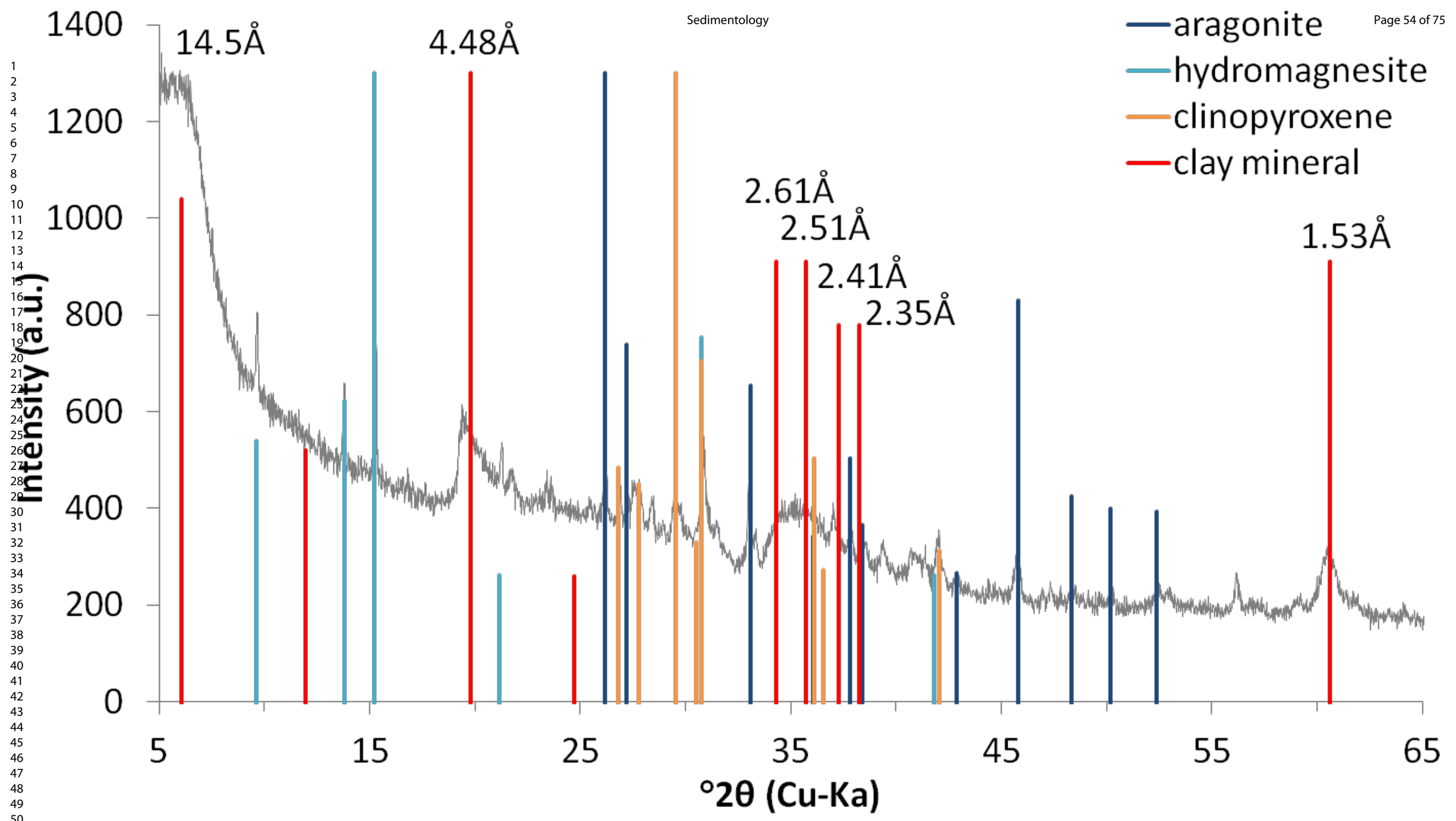
14.5Å
4.48Å
2.61Å
2.51Å
2.41Å
2.35Å
1.53Å
aragonite
hydromagnesite
clinopyroxene
clay mineral
Intensity (a.u.)
°2θ (Cu-Ka)
0
200
400
600
800
1000
1200
1400
5
15
25
35
45
55
65

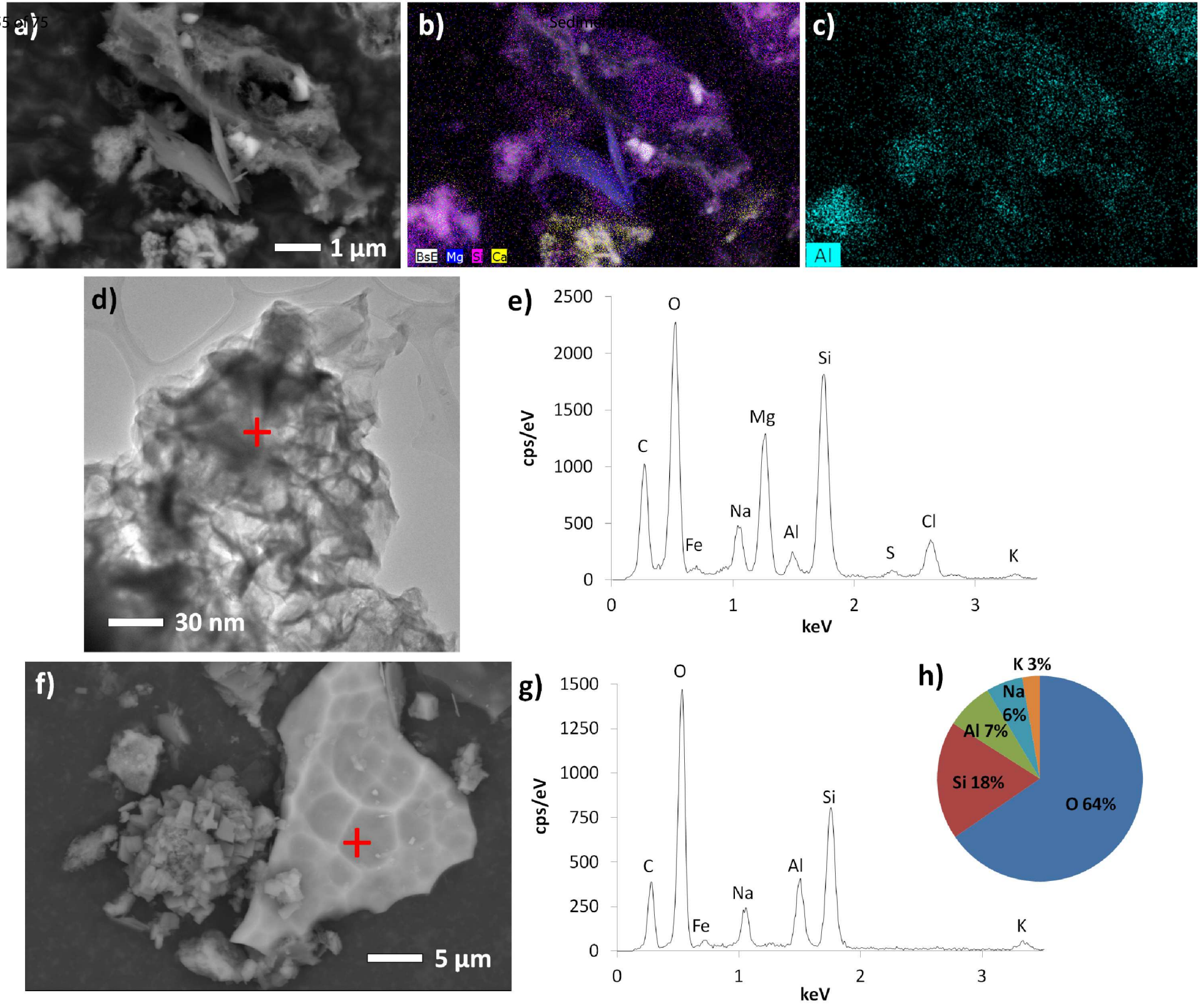
a)
1 µm
b)
BsE Mg Si Ca
c)
Al
d)
30 nm
e)
cps/eV
keV
O
Si
Mg
C
Na
Al
Fe
S
Cl
K
f)
5 µm
g)
cps/eV
keV
O
Si
C
Al
Na
Fe
K
h)
K 3%
Na 6%
Al 7%
Si 18%
O 64%

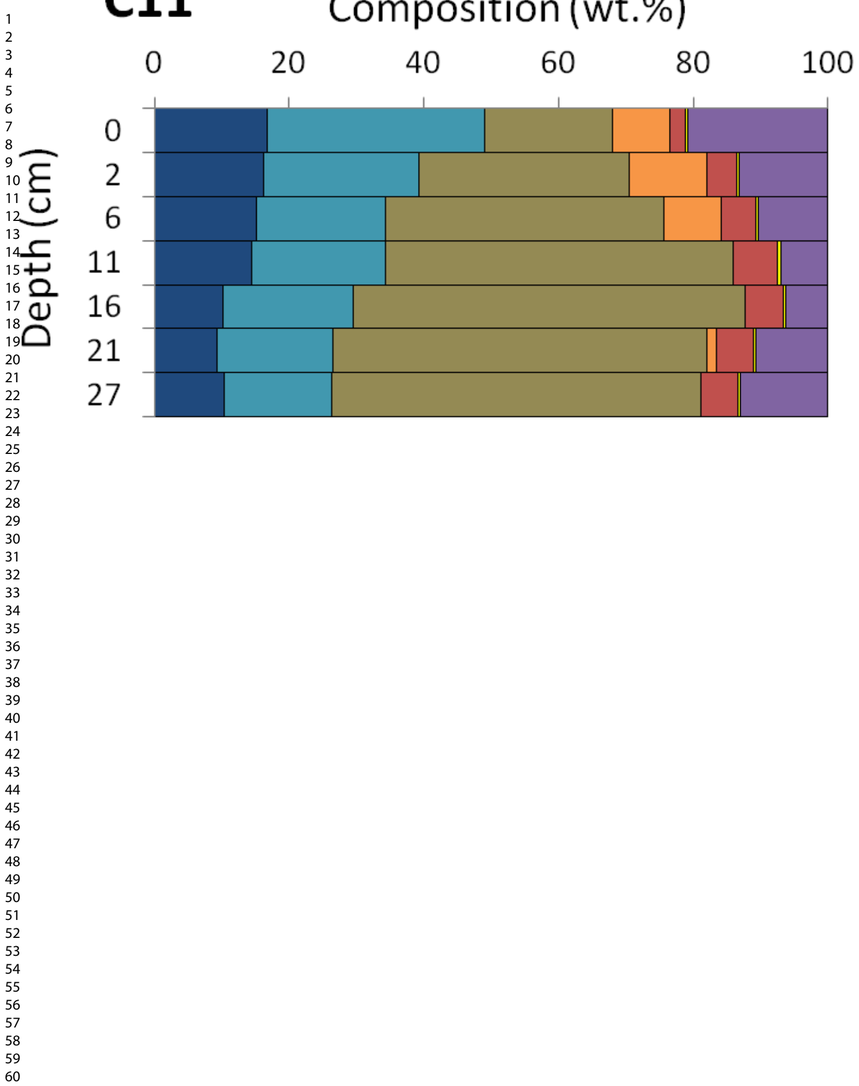
C11
Composition (wt.%)
0
20
40
60
80
100
Depth (cm)
0
2
6
11
16
21
27

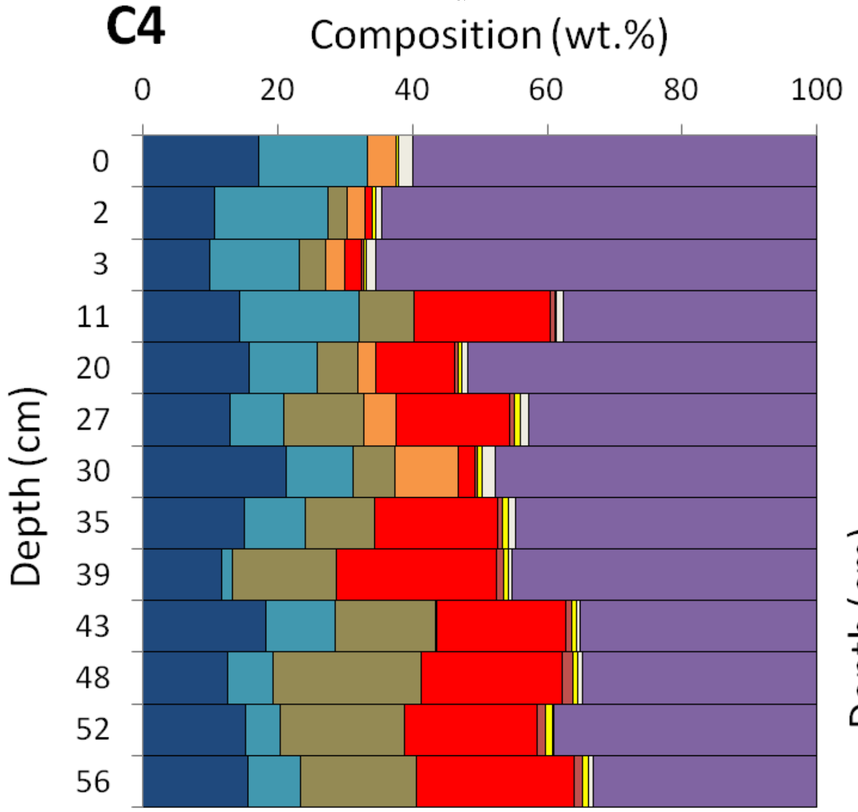
C4
Composition (wt.%)
0
20
40
60
80
100
Depth (cm)
0
2
3
11
20
27
30
35
39
43
48
52
56

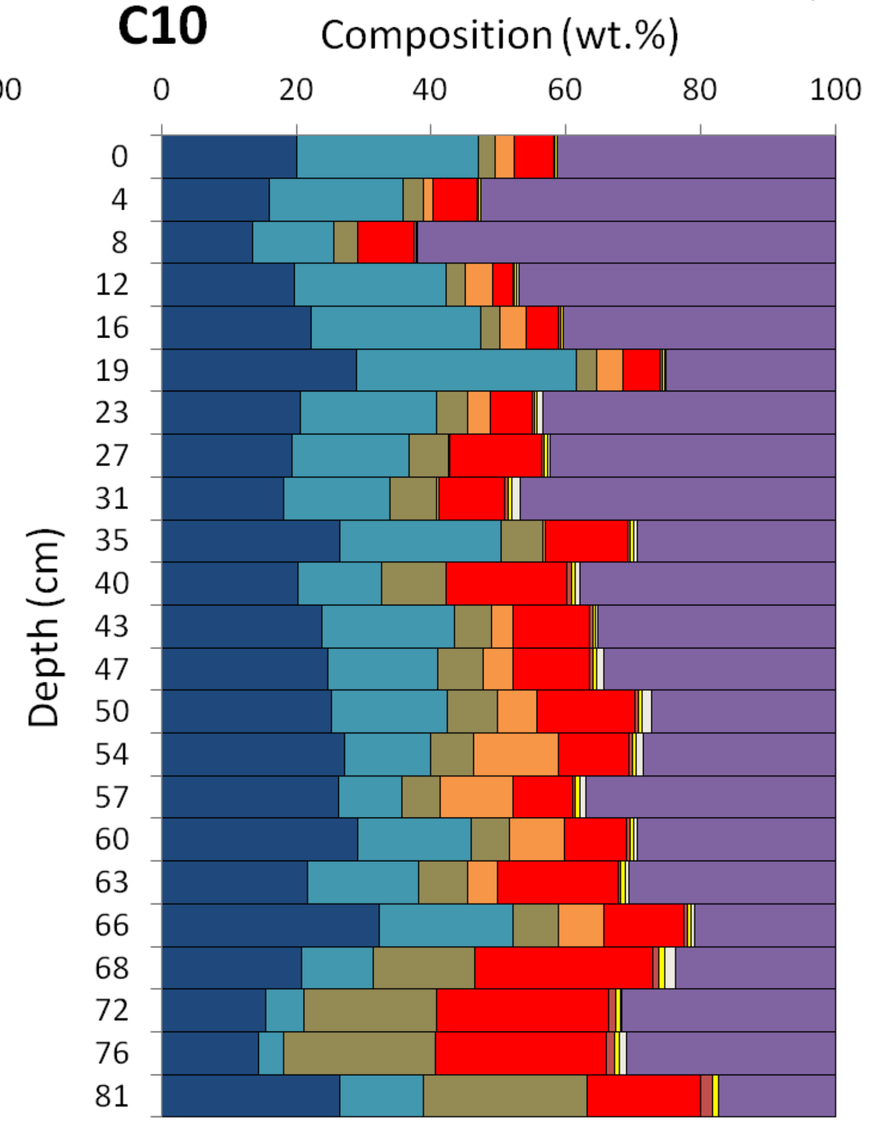
C10
Composition (wt.%)
0
20
40
60
80
100
Depth (cm)
0
4
8
12
16
19
23
27
31
35
40
43
47
50
54
57
60
63
66
68
72
76
81


Aragonite
Hydromagnesite
Alkaline feldspar
Clinopyroxene
Magnetite
Pyrite
Halite
Saponite
Organic matter

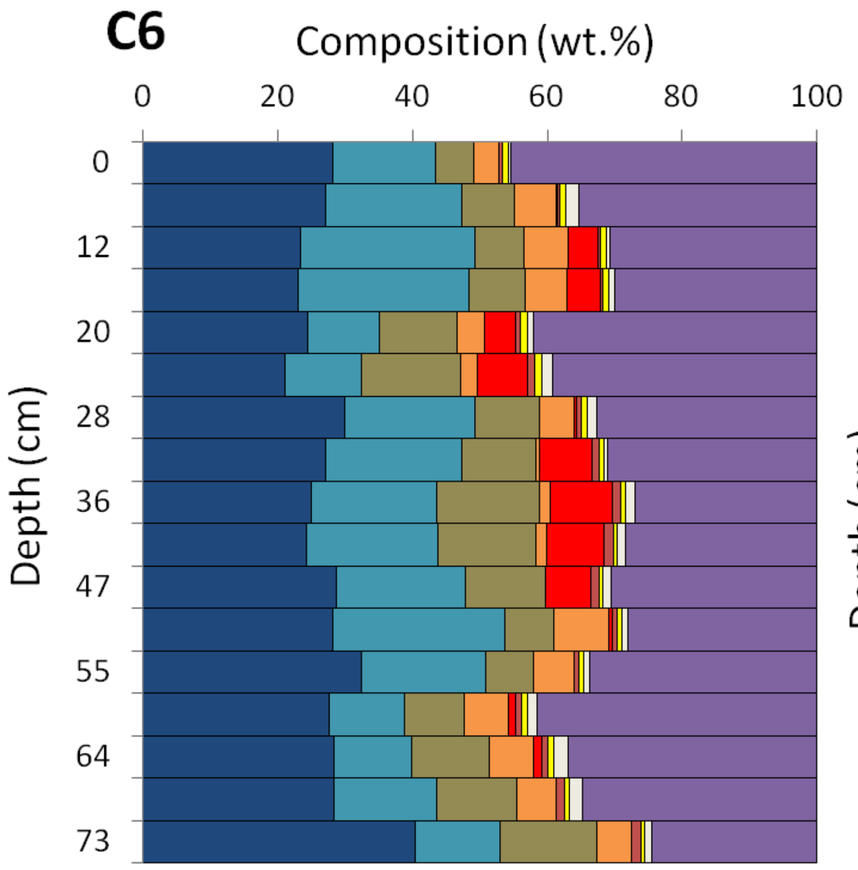
C6
Composition (wt.%)
0
20
40
60
80
100
Depth (cm)
0
12
20
28
36
47
55
64
73

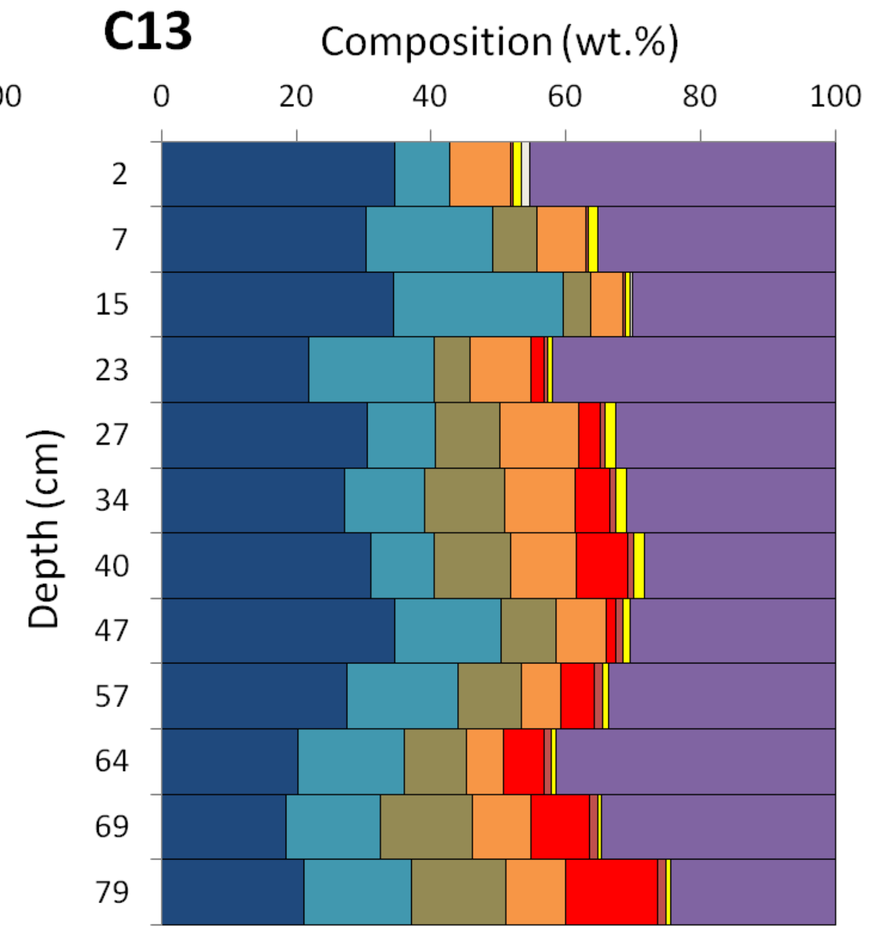
C13
Composition (wt.%)
0
20
40
60
80
100
Depth (cm)
2
7
15
23
27
34
40
47
57
64
69
79

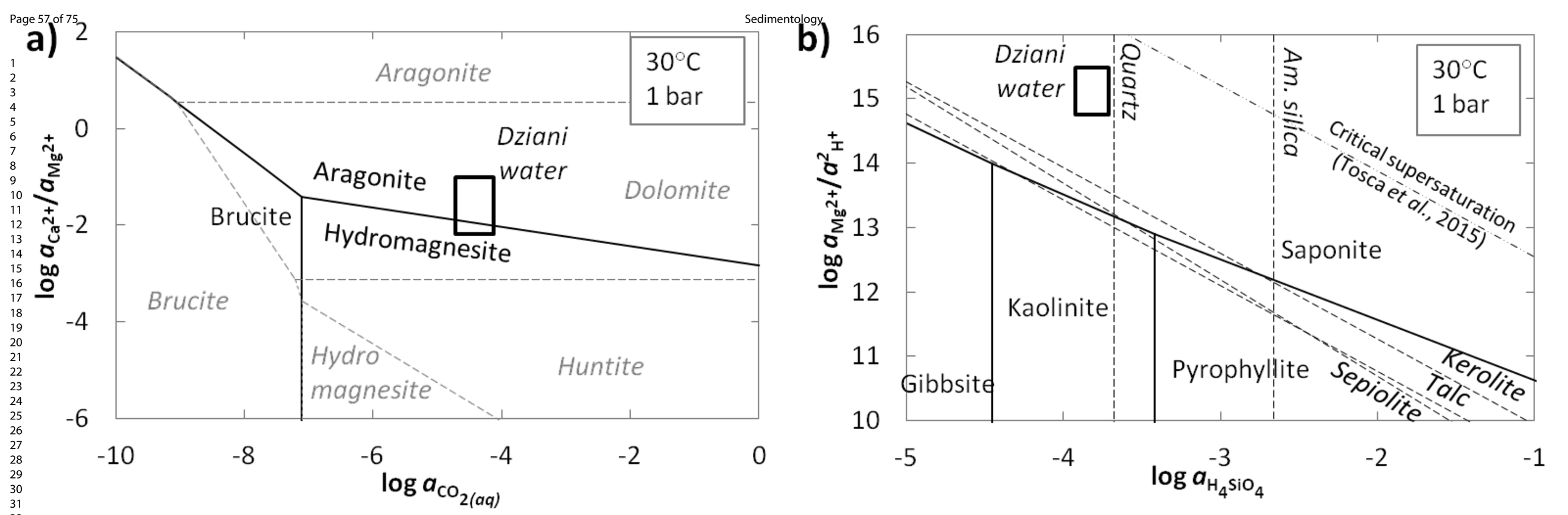
a)
30°C
1 bar
Aragonite
Dziani water
Aragonite
Brucite
Hydromagnesite
Dolomite
Brucite
Hydro magnesite
Huntite
log $a_{Ca^{2+}}/a_{Mg^{2+}}$
log $a_{CO_{2(aq)}}$
2
0
-2
-4
-6
-10
-8
-6
-4
-2
0
b)
30°C
1 bar
Dziani water
Quartz
Am. silica
Critical supersaturation (Tosca et al., 2015)
Saponite
Kaolinite
Gibbsite
Pyrophyllite
Kerolite
Talc
Sepiolite
log $a_{Mg^{2+}}/a^2_{H^+}$
log $a_{H_4SiO_4}$
16
15
14
13
12
11
10
-5
-4
-3
-2
-1

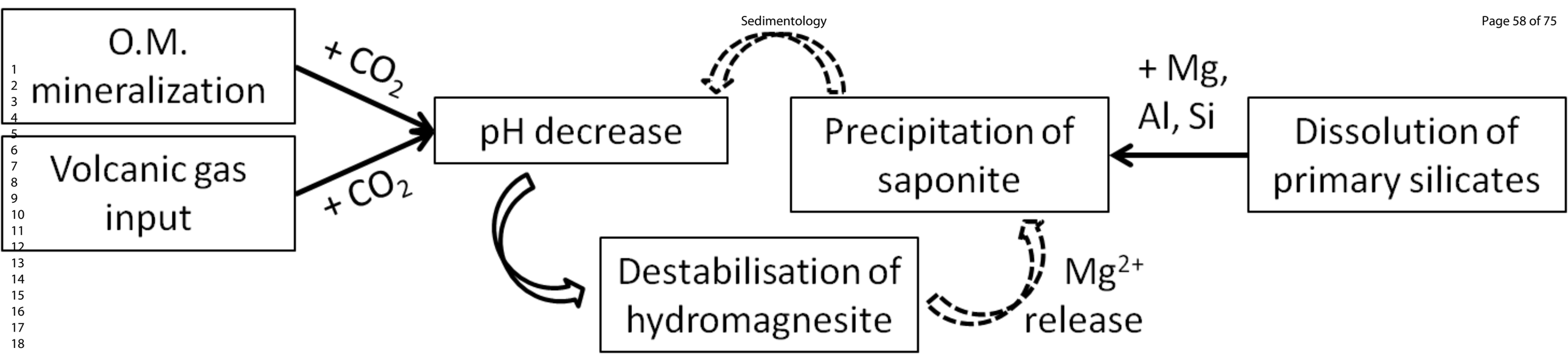
O.M. mineralization
Volcanic gas input
+ CO_2
+ CO_2
pH decrease
Precipitation of saponite
+ Mg, Al, Si
Dissolution of primary silicates
Destabilisation of hydromagnesite
Mg^{2+} release

Table 1. Method for quantification of mineral phases

Mineral	Chemical formula	Calculation*
Halite	NaCl	Halite = [Cl]
Alkaline feldspars	$Na_{0.7}K_{0.3}AlSi_3O_8$	Alk feld = [K]/0.3
Saponite	$K_{0.01}Mg_{0.12}Ca_{0.02}Na_{0.28}(Mg_{2.22}Fe_{0.18}Al_{0.28})(Si_{3.61}Al_{0.39})O_{10}(OH)_2$	Sap = ([Al]– Alk feld)/0.67
Clinopyroxene	$(Ca_yMg_{1-y})SiO_3$	Px = [Si]–3*Alk feld–3.61*Sap
Hydromagnesite	$Mg_5(CO_3)_4(OH)_2 \cdot (H_2O)_4$	Hydromag = ([Mg]–2.34*Sap –(1-*y*)*Px)/5
Aragonite	$CaCO_3$	Ara = ([Ca] –*y**Px-0.02*Sap)
Pyrite	FeS_2	Pyr = [S]/2
Magnetite	Fe_3O_4	Mag = ([Fe] – Pyr-0.18*Sap)/3

*[*X*] are the concentrations in mol.% of Cl, K, Al, Si, Mg, Ca, S and Fe measured with XRF.

Table 2. Refined composition of saponite in sediment core C4 (in weight %)

Sample	According to EPMA								According to exchanged cations			
	Al	Ca	Fe	K	Mg	Mn	Na	Si	Na	K	Ca	Mg
C4	3.65	0.20	2.01	0.07	11.62	0.07	0.70	20.78	0.65	0.02	0.04	0.15

SUPPORTING INFORMATION

Table A1. Sediment cores and rock samples of the Dziani Dzaha

Sample	GPS coordinates (degree min)	
	Latitude South	Longitude East
Sediment cores		
DZ12-4 C1	S 12°46.269’	E 45°17.288’
DZ12-4 C2	S 12°46.269’	E 45°17.288’
DZ14-4 C4	S 12°46.223’	E 45°17.275’
DZ14-10 C6	S 12°46.235'	E 45°17.392'
DZ14-10 C9	S 12°46.337’	E 45°17.310’
DZ14-10 C10	S 12°46.169’	E 45°17.265’
DZ14-10 C11	S 12°46.325’	E 45°17.425’
DZ16-8 C12	S 12°46.245'	E 45°17.335'
DZ16-8 C13	S 12°46.235'	E 45°17.392'
Volcanic catchment		
DZ14-10 R1	-	-
DZ14-10 R2	-	-
DZ14-10 R3	-	-
DZ14-10 R4	-	-
DZ14-10 R5	-	-
DZ14-10 R6	-	-
DZ16-8 R1	S 12°46.520'	E 45°17.472'
DZ16-8 R2	S 12°46.532'	E 45°17.475'
DZ16-8 R3	S 12°46.582'	E 45°17.365'
DZ16-8 R4	S 12°46.318'	E 45°17.537'
DZ16-8 R5	S 12°46.318'	E 45°17.537'
DZ16-8 R6	S 12°46.318'	E 45°17.537'

Table A2. Total carbon content and carbon isotope composition of the sediment cores

Depth (cm)	TC (wt %)	δ^{13}C TC (‰)	δ^{13}C TOC (‰)	δ^{13}C TIC (‰)	Calculated TOC (wt %)*	Calculated organic matter (wt.%)*
			DZ12-4 C1			
5 - 7,5	36.8	-15.6	-	-	38.8	73.7
7,5 - 8,5	40.0	-14.4	-	-	40.4	76.8
8,5 - 11	35.1	-14.2	-	-	35.3	67.1
-	29.9	-13.5	-	-	29.4	55.9
16 - 18	23.1	-14.9	-	-	23.8	45.3
18 - 22	17.4	-14.8	-	-	17.9	34.0
22 - 23	17.0	-15.0	-	-	17.5	33.3
23 - 28	29.4	-15.4	-	-	30.7	58.4
28 - 29	22.3	-16.0	-	-	23.8	45.1
29 - 34	20.5	-14.3	-	-	20.7	39.3
34 - 37	18.6	-13.6	-	-	18.3	34.8
37 - 40	19.5	-13.5	-	-	19.1	36.4
			DZ12-4 C2			
2,5 - 4,5	33.9	-14.8	-	-	34.9	66.2
4,5 - 7	14.0	-14.8	-	-	14.4	27.3
7 - 10,5	4.0	-17.8	-	-	4.6	8.7
10,5 - 14	3.1	-18.5	-	-	3.5	6.7
14 - 16,5	16.1	-14.9	-	-	16.6	31.5
16,5 - 20	19.1	-14.1	-	-	19.2	36.4
20 - 23,5	13.9	-14.2	-	-	14.0	26.7
23,5 - 27	13.1	-14.3	-	-	13.3	25.2
27 - 30	12.7	-15.2	-	-	13.2	25.1
			DZ14-4 C4			
0 - 1	35.2	-10.9	-	-	31.6	60.0
1 - 2	33.1	-	-	-	-	-
2 - 3	37.2	-11.4	-	-	34.0	64.6
3 - 7	39.0	-10.5	-	-	34.5	65.5
7 - 11	33.6	-	-	-	-	-
11 - 14	23.9	-8.8	-	-	19.8	37.6
14 - 16	31.2	-	-	-	-	-
16 - 20	29.9	-	-	-	-	-
20 - 24	23.5	-18.7	-	-	27.2	51.7
24 - 27	19.7	-	-	-	-	-
27 - 30	23.5	-12.7	-	-	22.5	42.8
30 - 35	28.6	-10.3	-	-	25.1	47.7
35 - 39	25.4	-11.8	-	-	23.5	44.7
39 - 43	24.7	-13.0	-	-	23.8	45.3
43 - 48	19.3	-12.7	-	-	18.5	35.1
48 - 52	18.6	-13.5	-	-	18.3	34.8
52 - 56	21.1	-13.3	-	-	20.6	39.1
56 - 60	17.4	-14.1	-	-	17.4	33.1
			DZ14-10 C6			
0 - 3	27.3	-10.3	-15.4	16.0	23.9	45.4
8.5 - 12	23.2	-8.0	-14.0	17.2	18.6	35.2
12 - 16	21.2	-6.9	-15.7	-	16.2	30.8
16 - 20	20.8	-6.8	-13.9	15.8	15.8	30.0
20 - 24	26.1	-9.4	-13.1	-	22.1	42.0
24 - 28	23.8	-10.0	-13.2	15.9	20.6	39.2
28 - 32	23.4	-5.9	-13.5	16.3	17.2	32.6
32 - 36	20.6	-7.8	-13.7	-	16.3	31.0
36 - 40	18.2	-7.4	-13.6	16.9	14.2	27.0
40 - 44	18.8	-7.7	-12.6	-	14.9	28.3
44 - 46.5	-	-	-14.2	-	-	-
46.5 - 51	19.7	-8.5	-14.4	-	16.1	30.5
51 - 55	20.1	-6.0	-12.0	-	14.8	28.0
55 - 59	22.7	-7.4	-14.3	-	17.7	33.6

59 - 64	24.9	-10.3	-15.1	-	21.8	41.5
64 - 69	22.5	-9.9	-15.0	-	19.4	36.9
69 - 73	21.9	-9.0	-14.8	-	18.3	34.7
73 - 78	17.6	-5.9	-12.9	-	12.8	24.4
			DZ14-10 C9			
10 - 14	8.1	-12.6	-14.9	16.3	7.8	14.7
14 - 20	4.7	-12.0	-14.1	-	4.4	8.4
20 - 24	10.7	-12.3	-13.9	-	10.1	19.2
29 - 32	10.8	-11.6	-13.6	-	9.9	18.9
32 - 36	12.7	-13.5	-13.9	-	12.5	23.8
36 - 39	11.7	-11.9	-14.2	-	10.8	20.6
39 - 42	10.9	-12.7	-13.7	-	10.4	19.7
42 - 46	10.0	-12.1	-13.3	-	9.4	17.8
46 - 50	9.4	-9.9	-12.6	-	8.1	15.4
50 - 54	8.6	-11.1	-12.5	-	7.8	14.8
54 - 58	7.1	-12.8	-14.3	-	6.8	13.0
58 - 62	6.7	-12.0	-14.0	-	6.2	11.8
62 - 68	4.9	-12.8	-16.3	-	4.7	8.9
68 - 73	7.4	-9.5	-15.0	-	6.3	11.9
73 - 78	7.9	-	-10.4	-	-	-
			DZ14-10 C10			
0 - 4	35.7	-2.2	-	-	21.7	41.2
4 - 8	38.0	-5.8	-	-	27.7	52.6
8 - 12	41.2	-7.8	-	-	32.7	62.1
12 - 16	36.9	-4.1	-	-	24.7	46.9
16 - 19	34.3	-2.6	-	-	21.2	40.4
19 - 23	29.3	2.4	-	-	13.3	25.2
23 - 27	36.5	-2.8	-	-	22.8	43.4
27 - 31	32.3	-4.7	-	-	22.3	42.3
31 - 35	35.8	-4.7	-	-	24.7	46.9
35 - 39.5	32.1	1.5	-	-	15.5	29.4
39.5 - 43	28.4	-5.1	-	-	19.9	37.9
43 - 47	31.3	-1.7	-	-	18.5	35.2
47 - 50	28.0	-3.4	-	-	18.1	34.4
50 - 54	23.3	-2.5	-	-	14.4	27.3
54 - 57	24.9	-2.0	-	-	15.0	28.5
57 - 60	29.6	-3.8	-	-	19.5	37.1
60 - 63	29.9	0.5	-	-	15.5	29.4
63 - 66	25.4	-3.0	-	-	16.1	30.7
66 - 68	23.1	1.7	-	-	11.0	20.9
68 - 72	18.9	-3.9	-	-	12.5	23.8
72 - 76	24.0	-4.9	-	-	16.7	31.8
76 - 81	20.9	-7.4	-	-	16.3	30.9
81 - 86	15.9	-1.3	-	-	9.1	17.3
			DZ14-10 C11			
0 - 2	27.6	4.1	-	-	11.0	20.8
2 - 6	15.0	2.1	-	-	6.9	13.1
6 - 11	10.7	0.9	-	-	5.4	10.3
11 - 16	8.6	3.3	-	-	3.6	6.9
16 - 21	7.5	2.9	-	-	3.3	6.2
21 - 27	9.5	-1.7	-	-	5.6	10.7
27 - 33	10.8	-3.0	-	-	6.8	12.9

TC, TOC and TIC are for total carbon, total organic carbon and total inorganic carbon, respectively.
* See section "Material and Method" for details on the calculation

Table A3. Chemical composition of the mineral content of sediment cores

Depth (cm)	Na (wt.%)	Mg (wt.%)	Al (wt.%)	Si (wt.%)	S (wt.%)	Cl (wt.%)	K (wt.%)	Ca (wt.%)	Fe (wt.%)
DZ14-4 C4									
0-1	11.9	54.3	0.4	0.4	0.1	0.3	0.0	1.2	0.0
2-3	9.0	57.8	0.9	0.8	0.1	0.1	0.0	0.8	0.0
3-7	11.0	50.2	1.1	1.1	0.1	0.2	0.0	0.8	0.0
7-11	6.5	53.9	1.9	1.1	0.0	0.1	0.0	0.9	0.0
11-14	6.9	43.9	3.2	2.0	0.0	0.1	0.0	0.7	0.1
14-16	7.6	42.1	2.8	1.6	0.1	0.1	0.0	1.0	0.1
16-20	7.4	50.5	1.3	1.1	0.1	0.1	0.0	1.1	0.0
20-24	7.9	37.4	2.3	2.2	0.1	0.1	0.0	1.1	0.1
24-27	7.7	36.3	1.9	2.5	0.1	0.1	0.0	1.1	0.1
27-30	8.6	32.8	2.8	3.0	0.1	0.1	0.1	0.7	0.1
30-35	10.5	37.7	1.1	1.7	0.1	0.2	0.0	1.3	0.1
35-39	8.3	32.2	3.0	2.8	0.1	0.1	0.1	1.0	0.1
39-43	7.9	26.1	4.5	3.7	0.1	0.1	0.1	0.9	0.2
43-48	7.3	30.0	3.6	3.2	0.1	0.1	0.1	1.0	0.1
48-52	8.5	26.0	4.1	3.8	0.1	0.1	0.1	0.7	0.1
52-56	7.1	24.9	4.5	4.0	0.1	0.0	0.1	1.0	0.2
56-60	7.9	28.7	3.8	3.4	0.1	0.1	0.1	0.9	0.1
DZ14-10 C6									
0 - 3	7.6	39.8	1.1	1.1	0.1	0.0	0.0	2.0	0.1
3 - 6.5	8.6	36.6	2.4	1.8	0.1	0.1	0.1	1.3	0.1
8.5 - 12	11.0	43.5	1.0	1.1	0.1	0.2	0.0	1.3	0.0
12 - 16	6.2	50.3	1.8	1.3	0.1	0.0	0.0	1.0	0.0
16 - 20	7.2	48.5	1.8	1.3	0.1	0.1	0.0	1.0	0.1
20 - 24	11.4	30.4	1.7	2.1	0.2	0.1	0.1	1.6	0.1
24 - 28	11.5	28.8	2.1	2.4	0.1	0.2	0.1	1.3	0.1
28 - 32	10.1	39.4	1.3	1.2	0.1	0.1	0.1	1.6	0.1
32 - 36	7.0	39.0	2.5	1.7	0.1	0.1	0.1	1.5	0.1
36 - 40	8.9	34.8	2.4	2.1	0.1	0.1	0.1	1.2	0.1
40 - 44	8.9	36.5	2.4	2.0	0.1	0.1	0.1	1.2	0.1
44 - 46.5	8.4	22.8	4.0	3.4	0.1	0.1	0.2	1.5	0.2
46.5 - 51	8.3	35.9	2.2	1.7	0.1	0.1	0.1	1.6	0.1
51 - 55	6.3	49.3	1.4	1.1	0.1	0.1	0.0	1.3	0.1
55 - 59	7.7	41.0	1.1	1.2	0.1	0.1	0.0	1.8	0.1
59 - 64	10.1	32.3	1.3	1.7	0.1	0.2	0.1	1.8	0.1
64 -69	11.3	30.6	1.4	1.9	0.1	0.2	0.1	1.7	0.1
69 - 73	11.5	34.1	1.3	1.6	0.1	0.2	0.1	1.6	0.1
73 - 76	8.7	26.6	1.8	2.0	0.1	0.1	0.1	2.5	0.1
DZ14-10 C9									
0 - 3	0.0	73.2	7.6	0.5	0.0	0.0	0.0	0.6	0.0
6 - 10	0.0	83.9	11.1	0.4	0.0	0.0	0.0	0.2	0.0
10 - 14	4.2	59.7	6.2	1.2	0.0	0.1	0.1	0.2	0.1
14 - 20	5.9	27.9	8.0	3.9	0.1	0.0	0.2	0.3	0.2
20 - 24	2.6	64.6	5.5	1.1	0.0	0.0	0.0	0.4	0.0
24 - 28	2.5	58.3	3.7	1.4	0.0	0.0	0.0	0.6	0.0
28 - 32	3.8	46.0	4.6	2.2	0.0	0.0	0.0	0.7	0.1
32 - 36	3.7	50.0	2.5	1.8	0.0	0.0	0.0	0.9	0.0
36 - 39	0.0	59.9	6.8	1.3	0.0	0.0	0.0	0.7	0.0
39 - 42	2.9	54.5	3.5	1.5	0.0	0.0	0.0	0.8	0.0
42 - 46	2.4	61.8	4.5	1.1	0.0	0.0	0.0	0.6	0.0
46 - 50	0.0	60.7	17.0	1.3	0.0	0.0	0.0	0.4	0.0
50 - 54	2.4	44.5	10.0	2.5	0.0	0.0	0.0	0.3	0.1
54 - 58	2.7	41.2	9.0	2.9	0.0	0.0	0.1	0.4	0.1
58 - 62	3.1	34.3	8.5	3.6	0.1	0.0	0.1	0.5	0.1
62 - 68	4.4	16.1	9.8	8.0	0.1	0.0	0.2	0.2	0.2
68 - 73	4.0	22.6	8.4	5.9	0.1	0.0	0.1	0.5	0.2
73 - 78.5	3.5	26.7	7.9	4.5	0.1	0.0	0.1	0.9	0.1

DZ14-10 C10									
0-4	0.0	58.8	7.4	0.9	0.0	0.0	0.0	1.0	0.0
4-8	2.4	54.6	3.6	1.1	0.0	0.0	0.0	1.1	0.0
8-12	1.9	47.1	6.0	1.5	0.0	0.0	0.0	1.3	0.1
12-16	4.4	56.0	1.5	0.9	0.0	0.0	0.0	1.2	0.0
16-19	0.0	56.4	6.5	1.0	0.0	0.0	0.0	1.2	0.0
19-23	2.4	57.1	2.3	0.8	0.0	0.0	0.0	1.3	0.0
23-27	5.9	49.5	1.8	1.2	0.0	0.1	0.0	1.2	0.0
27-31	4.9	43.7	3.2	1.8	0.1	0.0	0.0	1.2	0.1
31-35	8.1	41.4	2.2	1.6	0.1	0.2	0.1	1.1	0.1
35-39.5	4.7	46.4	2.8	1.4	0.0	0.1	0.0	1.3	0.1
39.5-43	6.1	36.9	3.6	2.2	0.1	0.1	0.1	1.2	0.1
43-47	4.2	45.4	2.9	1.6	0.0	0.0	0.0	1.3	0.1
47-50	6.7	41.1	2.1	1.8	0.1	0.1	0.0	1.3	0.1
50-54	6.6	40.7	2.3	2.0	0.1	0.1	0.0	1.2	0.1
54-57	6.1	40.0	1.9	2.1	0.1	0.1	0.0	1.3	0.1
57-60	6.5	37.3	1.8	2.2	0.1	0.1	0.0	1.5	0.1
60-63	5.1	42.1	2.1	1.8	0.1	0.1	0.0	1.5	0.1
63-66	5.3	41.4	3.0	2.2	0.1	0.0	0.0	1.0	0.1
66-68	4.6	42.3	2.4	1.7	0.1	0.0	0.0	1.5	0.1
68-72	7.9	31.3	3.3	2.9	0.1	0.1	0.1	1.0	0.1
72-76	6.4	27.1	5.0	3.9	0.1	0.0	0.1	0.9	0.1
76-81	8.5	24.0	4.2	4.1	0.1	0.1	0.2	0.8	0.1
81-86	5.8	25.4	4.6	3.9	0.1	0.0	0.1	1.4	0.1
DZ14-10 C11									
0-2	3.4	47.2	6.5	1.9	0.0	0.0	0.1	0.6	0.1
2-6	4.2	33.8	7.6	3.2	0.0	0.0	0.1	0.6	0.2
6-11	5.6	26.0	7.0	4.2	0.0	0.0	0.2	0.6	0.2
11-16	6.5	19.8	6.4	5.2	0.1	0.0	0.3	0.7	0.3
16-21	7.1	18.4	6.5	5.8	0.0	0.0	0.3	0.5	0.3
21-27	6.3	18.1	7.3	6.1	0.0	0.0	0.3	0.4	0.3
27-30	6.9	16.2	6.9	6.4	0.0	0.0	0.3	0.5	0.3
DZ16-8 C13									
2-3cm	13.8	34.1	0.5	0.8	0.1	0.2	0.1	2.2	0.1
7-11	6.2	43.3	1.2	1.2	0.2	0.0	0.0	1.7	0.1
15-20	5.3	49.7	0.8	0.7	0.1	0.0	0.0	1.8	0.0
22.5-25	5.3	48.6	1.6	1.4	0.1	0.0	0.0	1.2	0.1
27-30.5	8.6	33.8	1.5	2.1	0.2	0.0	0.1	1.7	0.1
34-38	7.4	34.6	2.1	2.3	0.2	0.0	0.1	1.4	0.1
40-43	6.6	31.5	2.3	2.5	0.2	0.0	0.1	1.7	0.1
47-51	5.8	37.4	1.8	1.6	0.1	0.0	0.1	2.0	0.1
57-60	4.4	38.8	2.9	1.9	0.1	0.0	0.1	1.6	0.1
63.5-66	4.0	41.0	3.5	2.1	0.1	0.0	0.1	1.2	0.1
68.5-74	5.3	37.8	3.5	2.7	0.1	0.0	0.1	1.0	0.1
79-85	3.1	38.2	5.0	2.8	0.1	0.0	0.1	1.0	0.1
90.5-94	1.0	47.7	3.9	1.4	0.1	0.0	0.0	1.5	0.1
97.5-101	5.2	26.4	2.9	3.2	0.2	0.0	0.1	2.1	0.1
105-106	4.4	26.9	3.4	3.6	0.1	0.0	0.1	1.9	0.1

Table A4. Characterization and semi-quantification of mineral phases in the sediment cores with XRPD

Depth (cm)	Aragonite (wt.%)	Hydro-magnesite (wt.%)	Alkaline feldspar (wt.%)	Clino-pyroxene* (wt.%)	Quartz (wt.%)	Calcite (wt.%)	Dolomite (wt.%)	Magnesite (wt.%)	Magnetite (wt.%)	Pyrite (wt.%)	Halite (wt.%)	Clay**
DZ12-4 C2												
0-2.5	30	50	-	15	-	-	-	-	-	-	5	-
-2.5-4.5	31	63	-	-	-	-	-	-	-	-	6	-
4.5-7	49	33	-	18	-	-	-	-	-	-	-	D
7-10.5	-	-	49	-	16	35	-	-	-	-	-	-
10.5-14	-	-	67	-	-	33	-	-	-	-	-	-
14-16.5	43	33	-	20	-	-	-	-	-	-	4	D
16.5-20	71	-	-	-	-	-	-	-	20	-	9	D
20-23.5	76	-	-	-	-	-	-	-	14	-	10	D
23.5-27	100	-	-	-	-	-	-	-	-	-	-	D
27-30	100	-	-	-	-	-	-	-	-	-	-	D
DZ14-4 C4												
0-1	39	43	-	14	-	-	-	-	-	-	4	-
1-2	42	58	-	-	-	-	-	-	-	-	-	-
2-3	37	53	-	10	-	-	-	-	-	-	-	-
3-7	44	43	-	13	-	-	-	-	-	-	-	-
7-11	46	45	-	10	-	-	-	-	-	-	-	D
11-14	50	38	-	12	-	-	-	-	-	-	-	-
14-16	57	33	-	10	-	-	-	-	-	-	-	D
16-20	54	35	-	11	-	-	-	-	-	-	-	-
20-24	70	17	-	13	-	-	-	-	-	-	-	D
24-27	93	-	-	-	-	-	-	-	7	-	-	D
27-30	88	-	-	-	-	-	-	-	12	-	-	D
30-35	72	21	-	-	-	-	-	-	-	-	7	-
35-39	89	-	-	-	-	-	-	-	11	-	-	D
39-43	99	-	-	-	-	-	-	-	-	-	-	-
43-48	96	-	-	-	-	-	-	-	4	-	-	D
48-52	100	-	-	-	-	-	-	-	-	-	-	D
52-56	94	-	-	-	-	-	-	-	5	-	-	-
56-60	93	-	-	-	-	-	-	-	6	-	-	D
DZ14-10 C6												
0-3	65	24	-	11	-	-	-	-	-	-	-	-
3-8.5	-	-	-	-	-	-	-	-	-	-	-	-
8.5-12	66	26	-	8	-	-	-	-	-	-	-	-
12-16	54	32	-	15	-	-	-	-	-	-	-	-
16-20	49.0	40	-	11	-	-	-	-	-	-	-	-
20-24	84	-	-	-	-	-	-	-	6	-	10	-
24-28	84	-	-	-	-	-	-	-	16	-	-	-
28-32	57	26	-	-	5	-	12	-	-	-	-	-
32-36	54	32	-	-	5	-	9	-	-	-	-	-
36-40	70	20	-	-	7	-	3	-	-	-	-	-
40-44	64	23	-	-	5	-	4	-	-	-	4	-
44-46	70	19	-	-	8	-	3	-	-	-	-	-
46-51	59	25	-	-	6	-	10	-	-	-	-	-
51-55	55	29	-	-	3	-	13	-	-	-	-	-
55-59	37	30	-	33	-	-	-	-	-	-	-	-
59-64	72	13	-	-	9	-	6	-	-	-	-	-
64-69	57	22	-	-	16	-	-	-	-	-	5	-
69-73	77	17	-	-	6	-	-	-	-	-	-	-
73-76	55	29	-	-	12	-	-	-	-	-	4	-
DZ14-10 C9												
6-10	6	73	-	16	-	-	-	5	-	-	-	-
10-14	-	55	-	11	-	-	-	34	-	-	-	-

14-20	-	-	-	-	-	-	-	-	-	-	-	-
20-24	29	58	-	13	-	-	-	-	-	-	-	D
24-28	13	73	-	14	-	-	-	-	-	-	-	-
29-32	42	49	-	-	-	-	-	-	9	-	-	D
32-36	49	40	-	11	-	-	-	-	-	-	-	D
36-39	34	49	-	17	-	-	-	-	-	-	-	-
39-42	36	51	-	13	-	-	-	-	-	-	-	D
42-46	28	54	-	18	-	-	-	-	-	-	-	D
46-50	21	64	-	15	-	-	-	-	-	-	-	D
50-54	17	64	-	19	-	-	-	-	-	-	-	D
54-58	31	69	-	-	-	-	-	-	-	-	-	D
58-62	55	45	-	-	-	-	-	-	-	-	-	D
62-68	-	-	-	-	49	-	-	-	-	51	-	-
68-73	46	-	-	-	-	-	33	-	-	21	-	D
73-78.5	40	-	-	-	-	-	53	-	-	7	-	-
DZ14-10 C10												
0-4	37	51	-	12	-	-	-	-	-	-	-	-
4-8	40	46	-	14	-	-	-	-	-	-	-	-
8-12	45	44	-	12	-	-	-	-	-	-	-	-
12-16	40	45	-	15	-	-	-	-	-	-	-	-
16-19	40	42	-	18	-	-	-	-	-	-	-	-
19-23	42	42	-	15	-	-	-	-	-	-	-	-
23-27	53	39	-	8	-	-	-	-	-	-	-	-
27-31	60	29	-	11	-	-	-	-	-	-	-	-
31-35	53	34	-	14	-	-	-	-	-	-	-	-
35-39.5	54	33	-	13	-	-	-	-	-	-	-	-
39.5-43	58	27	-	15	-	-	-	-	-	-	-	-
43-47	60	30	-	10	-	-	-	-	-	-	-	-
47-50	71	21	-	8	-	-	-	-	-	-	-	-
50-54	65	22	-	13	-	-	-	-	-	-	-	-
54-57	68	18	-	14	-	-	-	-	-	-	-	-
57-60	84	11	-	-	5	-	-	-	-	-	-	-
60-63	69	22	-	9	-	-	-	-	-	-	-	-
63-66	61	26	-	13	-	-	-	-	-	-	-	D
66-68	70	24	-	6	-	-	-	-	-	-	-	-
68-72	92	-	-	-	-	-	-	-	8	-	-	D
72-76	83	-	-	-	-	-	8	-	9	-	-	-
76-81	100	-	-	-	-	-	-	-	-	-	-	-
81-86	68	-	-	-	7	-	-	-	-	25	-	-
DZ14-10 C11												
0-2	33	50	-	17	-	-	-	-	-	-	-	-
2-6	24	21	55	-	-	-	-	-	-	-	-	-
6-11	19	-	81	-	-	-	-	-	-	-	-	-
11-16	8	-	92	-	-	-	-	-	-	-	-	-
16-21	14	-	86	-	-	-	-	-	-	-	-	-
21-27	17	-	83	-	-	-	-	-	-	-	-	-
27-33	15	-	85	-	-	-	-	-	-	-	-	-
DZ16-8 C13												
0-2	68	32	-	-	-	-	-	-	-	-	-	-
2-3	84	16	-	-	-	-	-	-	-	-	-	-
3-4	66	34	-	-	-	-	-	-	-	-	-	-
4-5	48	39	-	13	-	-	-	-	-	-	-	-
5-6	47	43	-	11	-	-	-	-	-	-	-	-
6-7	47	42	-	11	-	-	-	-	-	-	-	-
7-8	41	50	-	9	-	-	-	-	-	-	-	-
7-11	58	29	-	13	-	-	-	-	-	-	-	-
11-15	66	24	-	10	-	-	-	-	-	-	-	-
15-20	61	29	-	10	-	-	-	-	-	-	-	-
20-22,5	53	34	-	13	-	-	-	-	-	-	-	-

22,5-25	62	28	-	10	-	-	-	-	-	-	-	-
25-27	43	57	-	-	-	-	-	-	-	-	-	-
27-30,5	98	-	-	-	2	-	-	-	-	-	-	-
30,5-34	81	9	-	-	10	-	-	-	-	-	-	-
34-38	89	-	-	-	11	-	-	-	-	-	-	-
38-40	69	26	-	-	5	-	-	-	-	-	-	-
40-43	91	-	-	-	9	-	-	-	-	-	-	-
43-47	95	-	-	-	5	-	-	-	-	-	-	-
47-51	75	20	-	-	5	-	-	-	-	-	-	-
51-57	75	21	-	-	4	-	-	-	-	-	-	-
57-60	41	54	-	-	4	-	-	-	-	-	-	-
60-63,5	86	6	-	-	8	-	-	-	-	-	-	-
63,5-66	72	28	-	-	-	-	-	-	-	-	-	-
66-68,5	67	21	-	-	12	-	-	-	-	-	-	-
68,5-74	45	55	-	-	-	-	-	-	-	-	-	-
74-79	45	55	-	-	-	-	-	-	-	-	-	-
79-85	59	27	-	14	-	-	-	-	-	-	-	-
85-90,5	57	27	-	16	-	-	-	-	-	-	-	-
90,5-94	61	27	-	12	-	-	-	-	-	-	-	-
94-97,5	77	19	-	4	-	-	-	-	-	-	-	-
97,5-101	86	6	-	-	8	-	-	-	-	-	-	-
101-105	89	-	-	-	11	-	-	-	-	-	-	-
105-106	91	-	-	-	9	-	-	-	-	-	-	-

*The XRPD patterns indicate alternatively the presence of diopside or clinoenstatite, which are referred here and in the text as clinopyroxene.

**D means that the clay mineral is detected in the sample. Clay minerals were not taken into account in the semi-quantification with the RIR method.

Table A5. Characterization and semi-quantification of mineral phases in samples of the volcanic catchment with XRPD

Sample	Description	Calcite (wt.%)	Alk. Feld. (wt.%)	Analcime (wt.%)	Cpx (wt.%)	Magnetite (wt.%)	Olivine (wt.%)	Volcanic glass
DZ14-10 R1	Volcanic pumice	-	95	-	-	5	-	x
DZ14-10 R2	Cm-size block in ash layers	66	34	-	-	-	-	-
DZ14-10 R3	Cm-size block in ash layers	67	33	-	-	-	-	-
DZ14-10 R4	Cm-size igneous rock in ash layers	-	-	20	72	8	-	-
DZ14-10 R5	Cm-size igneous rock in ash layers	-	15	49	36	-	-	-
DZ14-10 R6	Cm-size igneous rock in ash layers	-	32	-	55	-	13	-
DZ16-8 R1	Ash layers	45	55	-	-	-	-	x
DZ16-8 R2	Ash layers	51	49	-	-	-	-	x
DZ16-8 R3	Volcanic pumice	46	54	-	-	-	-	x
DZ16-8 R4	Volcanic pumice	100	-	-	-	-	-	x
DZ16-8 R5	Cm-size block in ash layers	100	-	-	-	-	-	-
DZ16-8 R6	Cm-size igneous rock in ash layers	-	-	48.5	46.5	5	-	-

x: the baseline strongly affected by noise suggests the predominance of volcanic glass in these samples

Table A6. Elemental composition of samples of the volcanic catchment

Sample	Na (mol.%)	Mg (mol.%)	Al (mol.%)	Si (mol.%)	S (mol.%)	Cl (mol.%)	K (mol.%)	Ca (mol.%)	Fe (mol.%)
				DZ16-8					
R2	7.4	1.6	17.7	51.8	0.0	0.3	6.1	8.9	5.6
R3	9.5	0.3	17.8	53.3	0.0	0.3	6.6	7.1	4.8
R4	13.3	0.4	17.4	53.5	0.1	0.8	6.6	3.0	4.5
R6	7.1	10.6	14.0	41.1	0.0	0.1	1.7	11.5	11.2

Table A7. Quantification of the sediment composition (organic matter and mineral phases including clays) in the sediment cores C4, C6, C10, C11 and C13

Depth (cm)	Halite (wt.%)	Alk. Feld. (wt.%)	Saponite-like mineral (wt.%)	Clinopyroxene (wt.%)	Hydromagnesite (wt.%)	Aragonite (wt.%)	Pyrite (wt.%)	Magnetite (wt.%)	O.M. (wt.%)
DZ14-4 C4									
0	2	0	0	4	16	17	0	0	60
2	1	3	1	3	17	11	0	0	65
3	1	4	2	3	13	10	0	0	66
11	1	8	20	0	18	14	0	1	38
20	1	6	12	3	10	16	1	0	52
27	1	12	17	5	8	13	1	1	43
30	2	6	3	9	10	21	1	0	48
35	1	10	18	0	9	15	1	1	45
39	0	15	24	0	2	12	1	1	45
43	0	15	19	0	10	18	1	1	35
48	1	22	21	0	7	13	1	1	35
52	0	18	20	0	5	15	1	1	39
56	1	17	23	0	8	16	1	1	33
DZ14-10 C6									
0	0	6	0	4	15	28	1	0	45
8.5	2	8	0	6	20	27	1	0	35
12	0	7	4	6	26	23	1	0	31
16	1	8	5	6	25	23	1	0	30
20	1	11	5	4	11	24	1	1	42
24	2	15	8	2	11	21	1	1	39
28	1	10	0	5	19	30	1	1	33
32	1	11	8	1	20	27	1	1	31
36	1	15	9	1	19	25	1	1	27
40	1	15	9	2	19	24	1	1	28
46.5	1	12	7	0	19	29	1	1	31
51	1	7	1	8	26	28	1	1	28
55	1	7	0	6	19	32	1	1	34
59	1	9	1	6	11	28	1	1	41
64	2	12	1	7	12	28	1	1	37
69	2	12	0	6	15	28	1	1	35
73	1	14	0	5	13	40	1	1	24
DZ14-10 C10									
0	0	3	6	3	27	20	0	0	41
4	0	3	7	1	20	16	0	0	53
8	0	4	8	0	12	13	0	0	62
12	0	3	3	4	22	20	0	0	47
16	0	3	5	4	25	22	0	0	40
19	0	3	6	4	32	29	0	0	25
23	1	4	6	3	20	21	0	0	43
27	0	6	14	0	17	19	0	0	42
31	1	7	10	0	16	18	0	0	47
35	1	6	12	0	24	27	0	0	29
39.5	1	10	18	0	12	20	1	1	38

43	0	6	11	3	20	24	0	0	35
47	1	7	11	5	16	25	1	1	34
50	1	8	14	6	17	25	1	1	27
54	1	6	10	13	13	27	1	0	28
57	1	6	9	11	9	26	1	0	37
60	1	6	9	8	17	29	1	1	29
63	1	7	18	4	17	22	1	0	31
66	1	7	12	7	20	32	1	1	21
68	2	15	26	0	11	21	1	1	24
72	0	20	26	0	6	15	1	1	32
76	1	23	25	0	4	14	1	1	31
81	0	24	17	0	12	26	1	2	17
DZ14-10 C11									
0	0	19	0	8	32	16	0	2	22
2	0	31	0	11	23	16	0	4	15
6	0	41	0	8	19	15	0	5	12
11	0	51	0	0	20	14	0	7	7
16	0	57	0	0	20	10	0	6	7
21	0	54	0	1	17	9	0	6	12
27	0	53	0	0	16	10	0	5	15
DZ16-8 C13									
2	1	0	0	9	8	35	1	0	45
7	0	7	0	7	19	30	1	0	35
15	0	4	0	5	25	34	1	0	30
22.5	0	5	2	9	19	22	1	0	42
27	0	10	3	12	10	31	2	1	33
34	0	12	5	10	12	27	1	1	31
40	0	11	8	10	9	31	2	1	28
47	0	8	1	7	16	35	1	1	31
57	0	9	5	6	17	28	1	1	34
63.5	0	9	6	5	16	20	1	1	41
68.5	0	14	9	9	14	18	0	1	35
79	0	14	14	9	16	21	1	1	24

Table A8. Chemical composition of the lake waters

Survey	pH	Total alkalinity	Mg	Ca	Si
2009[a,b]	9.1-9.4	177.2	3.1	0.33	0.21
2010		241.0	4.5	0.04	0.27
2011		230.3	3.9	0.04	0.25
Oct.2014[c]	9.2	258.9	4.7	0.05	0.23

Cation concentrations are in $mmol \cdot L^{-1}$ and total alkalinity in $mmol \cdot L^{-1}$ eq. CO_3^{2-}

[a]Data from Leboulanger *et al.* (2017), except for the dissolved silica concentration measured in this study according to the method of Strickland and Parson (1972), *i.e.* the colorimetry of the reduced silico-molybdic complex. Sensitivity is about 2 $\mu M \cdot L^{-1}$ and the precision of ±5%.

[b]Sampling at the end of rainy season

[c]Data from Gérard *et al.* (2018)

Section A1. Characterization of the volcanic catchment

The volcanic catchment is mostly made of volcanic pumices and ash layers (Fig. A1a), containing fragments of solid/igneous rocks of various sizes typically ranging from a few centimeters to several tens of centimeters (Fig. A1b). The XRPD and XRF analyses of volcanic pumices and ash layers indicate the presence of alkaline feldspars and calcite (see Table A6 and A7 for details). The baseline of XRPD patterns is strongly affected by noise, suggesting that volcanic glass is dominant in these samples. The solid blocks found in the ash layers which contain large amounts of calcite (>60wt.%) correspond to fragments of the coral reef, which surrounds the biggest island of Mayotte and has been crossed over by the phreatomagmatic eruption at the origin of the Dziani Dzaha. The igneous rocks are mostly made of alkaline feldspars, clinopyroxene, analcime, and minor amounts of olivine and magnetite.

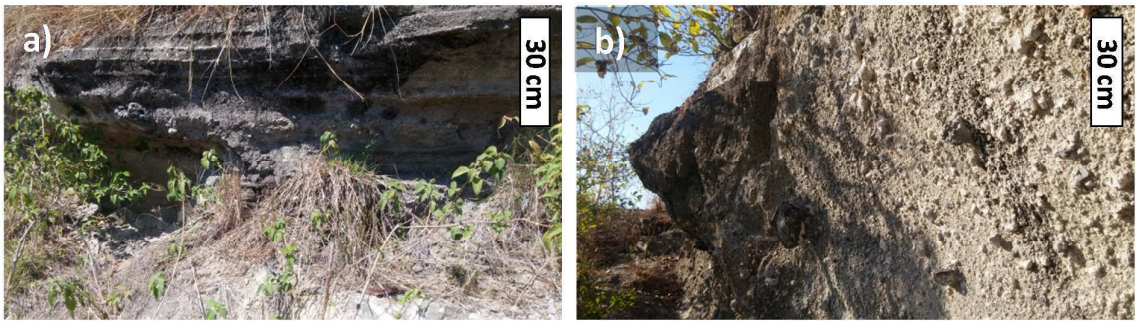

Figure A1. Volcanic catchment: (a) ash layers, (b) fragments of solid/igneous rocks in ash layers.

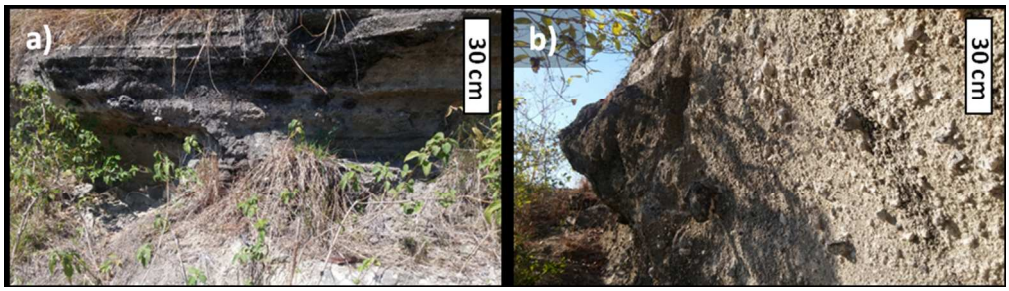

163x45mm (150 x 150 DPI)